NASA TECHNICAL NOTE

NASA TN D-6138

C. 1

NASA TN D-6138

AN ANALYTIC STUDY OF RADIATIVELY COOLED DELTA-WING STRUCTURES FOR HYPERSONIC AIRCRAFT

by James C. Robinson, Robert R. McWithey, and George F. Klich

Langley Research Center
Hampton, Va. 23365

NATIONAL AERONAUTICS AND SPACE ADMINISTRATION • WASHINGTON, D. C. • FEBRUARY 1971

1. Report No. NASA TN D-6138	2. Government Accession No.	3. Recipient's Catalog No.
4. Title and Subtitle AN ANALYTIC STUDY OF RADIATIVELY COOLED DELTA-WING STRUCTURES FOR HYPERSONIC AIRCRAFT		5. Report Date February 1971
		6. Performing Organization Code
7. Author(s) James C. Robinson, Robert R. McWithey, and George F. Klich		8. Performing Organization Report No. L-6666
		10. Work Unit No. 722-02-10-02
9. Performing Organization Name and Address NASA Langley Research Center Hampton, Va. 23365		11. Contract or Grant No.
		13. Type of Report and Period Covered Technical Note
12. Sponsoring Agency Name and Address National Aeronautics and Space Administration Washington, D.C. 20546		14. Sponsoring Agency Code

15. Supplementary Notes

16. Abstract

A thermal analysis and a stress and deflection analysis of five structural configurations for a radiatively cooled discrete delta wing were carried out by using design conditions characteristic of a Mach 8 research vehicle. The configurations included wing cover panels possessing either biaxial or uniaxial stiffness, support systems along the root chord or at two points on the root chord, and airfoil sections having either positive or negative camber.

Results indicate that for configurations supported along the full root chord, no excessive thermal or airload deformations occur. However, high thermal stresses occur in the wing cover panels that possess axial stiffness in the chordwise direction. Configurations in which the cover panels possess only spanwise axial stiffness exhibit significantly lower thermal stress in the panels but require that the rib caps carry larger thermal loads. The structural configuration possessing wing supports at only two locations along the root chord exhibited significant chordwise bowing as a result of the airloads plus inertia load and the temperature distribution in the structure. The magnitudes of the thermal loads were low, however, when compared with the thermal loads developed in the fully supported structural configurations. Changing the airfoil shape from positive to negative camber resulted in higher structural temperatures on the lower surface of the wing near the leading edge and generally higher thermal stresses in the structure.

17. Key Words (Suggested by Author(s)) Hypersonic vehicle wing, Hot structure, Aerodynamic heating, Structural analysis	18. Distribution Statement Unclassified – Unlimited

19. Security Classif. (of this report)	20. Security Classif. (of this page)	21. No. of Pages	22. Price*
Unclassified	Unclassified	64	$3.00

*For sale by the National Technical Information Service, Springfield, Virginia 22151

AN ANALYTIC STUDY OF RADIATIVELY COOLED DELTA-WING STRUCTURES FOR HYPERSONIC AIRCRAFT

By James C. Robinson, Robert R. McWithey,
and George F. Klich
Langley Research Center

SUMMARY

A thermal analysis and a stress and deflection analysis of five structural configurations for a radiatively cooled discrete delta wing were carried out by using design conditions characteristic of a Mach 8 research vehicle. The configurations included wing cover panels possessing either biaxial or uniaxial stiffness, support systems along the root chord or at two points on the root chord, and airfoil sections having either positive or negative camber.

Results indicate that for configurations supported along the full root chord, no excessive thermal or airload deformations occur. However, high thermal stresses occur in the wing cover panels that possess axial stiffness in the chordwise direction. Configurations in which the cover panels possess only spanwise axial stiffness exhibit significantly lower thermal stress in the panels but require that the rib caps carry larger thermal loads. The structural configuration possessing wing supports at only two locations along the root chord exhibited significant chordwise bowing as a result of the airloads plus inertia load and the temperature distribution in the structure. The magnitudes of the thermal loads were low, however, when compared with the thermal loads developed in the fully supported structural configurations. Changing the airfoil shape from positive to negative camber resulted in higher structural temperatures on the lower surface of the wing near the leading edge and generally higher thermal stresses in the structure.

INTRODUCTION

An aircraft flying at hypersonic speed in the earth's atmosphere will be subjected to aerodynamic heating, the magnitude of which depends upon the flight altitude and speed. To prevent this heating from damaging the structure of the aircraft, the structure may be protected by insulation and/or cooling or designed to withstand the resulting temperatures. In either of these approaches to the heating problem, temperature variations within the structure may occur and, if present, will produce thermal deformations and/or stresses.

This paper presents the results of an analytical study made to assess, on a preliminary basis, the severity of the problem for several types of wing structure subjected to a fixed set of aerodynamic conditions. In the study, the temperatures, stresses, and deformations in several configurations of a radiatively cooled hypersonic research aircraft wing were determined. The variations in the structural configurations studied included three types of structural cover panels, two methods of wing support, and two wing airfoil sections. The structural panels selected afforded a variation in surface smoothness, heat transfer, and stiffness characteristics. The wing support conditions provided a variation in the degree of root restraint and the airfoil sections provided a variation in the aerodynamic shape. The aerodynamic design conditions were those produced by a 4.5g Mach 8 turn in a given flight-velocity—altitude schedule. The analysis included the effects of aerodynamic heating and loading, radiation to space, and one-dimensional radiative and conductive heat transfer in the wing structure.

SYMBOLS

The units used for the physical quantities defined in this paper are given in both the U.S. Customary Units and in the International System of Units (SI) when applicable. Factors relating the two systems are given in reference 1 and in the appendix.

A_x cross-sectional area in the y,z plane resisting a force in x-direction

A_z shear area in the y,z plane resisting a force in z-direction

D_{ij} elements of material stiffness coefficient matrix

E Young's modulus

I_y moment of inertia about y-axis

I_z moment of inertia about z-axis

N element number

N_{gp} grid-point number

N_X, N_Y, N_{XY} stress resultants

T_m temperature of material

T_z temperature gradient in z-direction

$\bar{t}$ material volume per unit panel area

X,Y,Z overall rectangular coordinate system

x,y,z local rectangular coordinate system

$\epsilon_{xx}, \epsilon_{yy}, \epsilon_{zz}$ normal strain components

$\epsilon_{xy}, \epsilon_{xz}, \epsilon_{yz}$ shear strain components

$\sigma_{xx}, \sigma_{yy}, \sigma_{zz}$ normal stress components

$\sigma_{xy}, \sigma_{xz}, \sigma_{yz}$ shear stress components

$\delta_X, \delta_Y, \delta_Z$ deflections relative to overall coordinate axes X, Y, and Z, respectively

$\theta_X, \theta_Y, \theta_Z$ rotations relative to overall coordinate axes X, Y, and Z, respectively

VEHICLE GEOMETRY AND TRAJECTORY

The aerodynamic configuration selected for study was the rocket-powered hypersonic research vehicle shown in figure 1. The vehicle wing had a cross section with a flat bottom and a 0.75-inch-radius (1.91 cm) leading edge measured normal to the leading edge. The upper surface consisted of two conical surfaces separated by a flat surface in the center. This wing shape was used to study the effects of panel type and root support condition on temperatures, deformations, and stresses in the wing. Equations defining the aerodynamic surfaces (see sketch) are as follows:

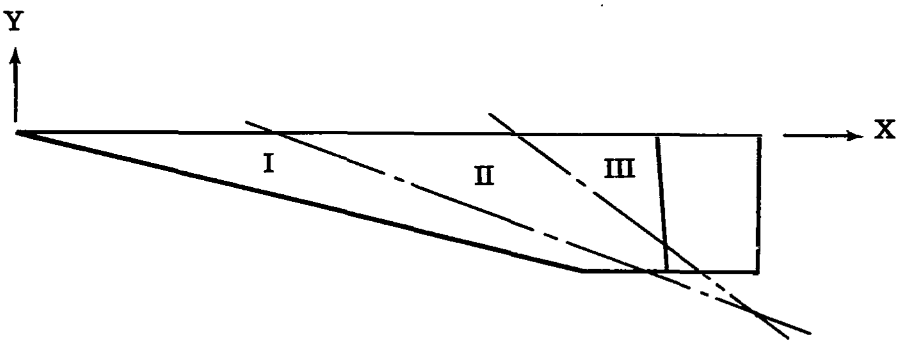

Top surface:

I $$0 = X^2 + 5.36206Y^2 + Z^2 + 5.3477XY - 278.437186X - 1135.6905Y + 1697.3812Z + 16.4885YZ - 1948.81176$$

II $$0 = 0.1077Y - Z + 12.4771$$

III $$0 = X^2 - 0.13164908Y^2 + Z^2 + 2.67386XY - 556.872166X - 1166.581354Y + 1841.734Z + 17.7106YZ + 54391.475$$

Bottom surface:

$$0 = Z$$

Leading edge:

$$0 = X^2 + 16.086362Y^2 + 17.0863608Z^2 + 8.0215615XY + 6.200348129X - 24.86823693Y - 25.62954461Z + 9.61107923$$

Planes defining tangent lines between:

1. Leading edge and bottom surface:

$$0 = 0.2419219X + 0.9702957Y - 0.75$$

2. Leading edge and I:

$$0 = 0.2419219X + 0.9702957Y - 0.331$$

3. I and II:

$$0 = X + 2.67385Y - 139.218593$$

4. II and III:

$$0 = X + 1.33693Y - 278.436083$$

The unit of length for the coordinates in these equations is inches. A right-hand coordinate system is used.

In order to study the structural effects of a change in camber similar to the aerodynamic study in reference 2, a configuration was analyzed identical to that shown in figure 1 except that the wing was in an inverted position. This change permits a direct evaluation of the temperature, deflection, and stress changes caused by the camber change for one combination of panel type and root support condition.

The flight-path variables used in the study (altitude, angle of attack, and velocity) are presented as functions of time in figure 2. Zero time occurs when the vehicle is air launched from a carrier aircraft. The powered portion of the flight consists of a pull-up maneuver, a climb to an altitude of about 83 000 feet (25 km) along a ballistic trajectory, and final acceleration to a Mach number of 8 with a resulting maximum dynamic pressure of 2200 psf (105 kN/m^2). The coasting portion of the flight consists of a 30-second-duration 4.5g turn and a glide to the landing area. In the turn, the combination of angle of attack, dynamic pressure, and inertia load produces a net wing loading on the positive camber wing of 140 psf (6.70 kN/m^2) which is used as the design value in the structural analyses.

STRUCTURAL CONFIGURATIONS

The arrangements of the structural components of the wings are shown in figure 3. The structure consists of a swept leading-edge beam, a rectangular grid of rib and spar beams, and structural cover panels. All beams were assumed to be composed of cap members and corrugated webs.

All structural elements were assumed to be made of René 41 (ref. 3), a nickel base super alloy with a nominal composition of Ni, 19% Cr, 11% Co, 10% Mo, 5% Fe, 3% Ti, and 1.5% Al. The elastic modulus, coefficient of thermal expansion, and tensile yield strength of this material at elevated temperatures are given in table I. It was assumed that this material could be used for structural application up to about 2060° R (1144 K).

The elevon was assumed to be actuated by a torque tube in the fuselage and supported at the fuselage and wing tip. The elevon was not considered in the analyses except for an elevon load at the wing tip equal to the simple beam reaction of the elevon for the same load intensity as that imposed upon the wing (that is, 140 psf (6.70 kN/m^2)). A summary of the structural configurations studied is presented in table II.

Cover Panels

Three structural cover-panel types were considered and are shown schematically in figure 4. The waffle panel (fig. 4(a)) consists of a flat sheet supported by two intersecting sets of integral ribs. It has biaxial stiffness, a smooth exterior surface, and provides the least resistance to radiative heat transfer through the wing depth. The beaded skin and circular-arc corrugation panel (fig. 4(b)) and the tubular panel (fig. 4(c)) have axial stiffness in only one direction and reduced shear stiffness, as compared with a flat sheet, because of the greater developed shear path length.

A single sheet exterior shield which has shallow corrugations in the chordwise direction was used with the tubular panel to provide a smoother aerodynamic surface. The tubular panel with its exterior surface provides three barriers to heat radiation through each wing surface.

The beaded-skin and circular-arc corrugation panel (fig. 4(b)) was used only in a chordwise orientation to avoid aerodynamic interaction with the wavy surface. The panel is structurally less efficient than the tubular panel but may be used in a chordwise orientation without the weight penalty of an additional aerodynamic surface. This panel provides two barriers to heat radiation through each wing surface.

Wing Fuselage Attachment

Two wing fuselage attachment methods were considered for transmitting loads between the wing and fuselage. One, called full support, had discrete attachments spaced along the full length of the wing root chord as shown in figure 3. The other system, called two-point support, had only two attachments on the root chord as shown in figure 3. At each attachment location there was a beam from the spar to the assumed upper attachment on the fuselage and a link from the lower spar cap to the assumed lower attachment on the fuselage. For configurations 1, 4, and 5, these beams were considered to be I-sections with wide flanges at the root rib tapering to a lug fitting at the fuselage to resist properly the spanwise stress resultant in the cover panels.

This arrangement provided resistance to wing spanwise bending moment and vertical and spanwise loads at each attachment location. The drag load was resisted by a diagonal beam for the full-support configurations and an assumed chordwise constraint at the aft attachment on the two-point-support configuration. Consequently, the differential movement between the wing and fuselage for the fully supported system consisted of chordwise expansion only. The two-point support system allowed differential chordwise expansion and bowing of the wing in its plane and normal to its plane.

The different combinations of structural cover panel, wing-fuselage attachment method, and airfoil orientation used for the structural configuration studies are shown in table II.

Structure Geometry

The geometric properties of the structures assumed for this analysis are given in tables III, IV, V, and figure 4. Table III gives the coordinates of grid points which are the locations of the intersections of the various structural members. Table IV gives the average properties of the beam members and the bounding grid-point numbers. Table V presents the stiffness properties of the cover panels. Figure 4 is a sketch of the cover panels and gives the sheet thicknesses used in the cover panels. The cover panels are considered to be minimum-gage construction. The corrugated shear webs in the beams in the wing were 0.012 inch (0.030 cm) thick with $\bar{t} = 0.016$ inch (0.041 cm) with the exception of the two spars at the support locations in configuration 3.

ANALYSES

Thermal Analysis

Temperatures within the wing structure were computed with a one-dimensional heat-transfer digital computer program. The program calculates aerodynamic heating rates to exposed surfaces from inputs consisting of a flight trajectory and corresponding ratios of local velocity to free-stream velocity, temperatures, densities, Mach numbers, and Reynolds numbers. It then computes transient temperature histories of the finite elements by a backward-differencing method. The effects of changes in element properties with temperature and radiation losses from the outer surfaces are included.

For these analyses, a turbulent boundary layer with an origin at the leading edge was assumed for all wing surfaces. The film heat-transfer coefficients used in the program to compute aerodynamic heating rates were those defined by Van Driest (refs. 4 and 5) with the Von Karman mixing length hypothesis. Free-stream conditions were based on the 1959 standard atmosphere tables (ref. 6) and the specific heat of air was allowed to vary with temperature. Inasmuch as the wing upper surface inclination to the flow was small, the ratios of local condition to free-stream condition needed as inputs to the computer program were computed by use of Prandtl-Meyer expansions. The ratios of local condition to free-stream condition for the lower surface were computed from pressure coefficients taken from chart 3 of reference 7. Radiative heat transfer through the wing panels as well as through the wing was established by use of the method for multiwalled sandwich panels outlined in reference 8. For the flight altitude-velocity schedule shown in figure 2, temperature histories were calculated at several points along a wing chord. These temperatures were then distributed over the complete wing by using the "strip" method of reference 9. Thus, detailed temperature distributions were developed for each structural configuration studied. These temperature distributions are for the original wing geometry and, hence, do not include the effects of structural deflections which result from air and thermal load.

Structural Analysis

The structural analysis of a hot delta wing such as those shown in figure 3 requires that spatial variation in member shape, material properties, and temperature be considered. In this study, the Structural Analysis and Matrix Interpretive System (SAMIS) (ref. 10) was used. SAMIS is a finite-element matrix displacement computer program that considers anisotropic material properties and material property variation with temperature.

To use a finite-element program, the structure must be idealized as an assembly of finite elements. The idealized model used is shown in figure 5. It has 150 plate elements and 119 beam elements. Deflection restraints were applied to the model at the wing-fuselage attachment points. A complete list of boundary restraints is given in table VI.

Program input data for each of the elements of the model includes its location, physical properties, average temperature, temperature change from a zero stress state, temperature gradients, and applied loading. Applied loads to the wing included the airloads plus inertia forces and the concentrated elevon load at the wing-tip elevon attachment point. (See fig. 3.) All applied loads were determined for the undeformed shape of the structure, consequently changes in applied loads and temperature caused by aerothermoelastic interaction are not included. Input data for each configuration are presented in tables III to VI. Information obtained from the program includes membrane stress resultants in the cover panels, loads and bending moments in the beams, and grid-point deflections.

RESULTS

Temperature Histories

Figure 6 presents temperature histories for the cover-panel surfaces at a location on the wing root rib 11.6 feet (3.54 meters) aft of the leading edge for configurations 1 to 5. (See table II.) This location is on the flat part of the wing. Figure 6(a) presents the temperature histories for configuration 1 which had waffle cover panels. Figure 6(b) presents the temperature histories for configurations 2 and 3 which used the beaded-skin and circular-arc corrugation panels. Figure 6(c) presents the temperature histories for configurations 4 and 5 which used tubular panels. The temperature histories for configuration 5 are the same as those for configuration 4 because the location chosen is on the flat section of the wing.

The time at which the maximum temperature in the lower cover panel occurred is shown by the dashed line in the figures. This time was selected as the design condition because the maximum structural temperature and near-maximum temperature gradient through the wing occurred at this time.

Temperature Distributions

As mentioned previously, the wing temperature distributions were developed by distributing chordwise temperature distributions over the wing by use of the strip method of reference 9. In configurations 2 to 5, where the structural cover panels were composed of two sheets of metal, the structural panel temperatures were taken to be the average of the temperatures of those two sheets.

Typical chordwise structural temperature distributions are presented in figure 7. Figure 7(a) presents a plot of the structural panel temperatures on the root-chord section of configurations 1, 2, and 3 at the design condition. Inasmuch as the temperatures on the forward part of the wing exceeded the assumed limiting temperature for the material (2060° R or 1144 K), the use of a variable conductance insulating material was assumed. The resulting temperatures are shown by the dashed lines in figure 7(a). Figures 7(b) and 7(c) present plots of the structural panel temperatures on the root-chord section of configuration 4 and configuration 5, respectively, at the design condition. The temperature in configuration 5 was allowed to exceed 2060° R (1144 K) so that a comparison could be made with configuration 4.

The temperature distributions used in the stress and deflection analysis are presented as isotherm plots in figures 8, 9, and 10. These figures show the temperatures of the lower structural panels in part (a) and the upper structural panels in part (b) for configurations 1 to 3, configuration 4, and configuration 5. The corresponding beam temperatures and temperature gradients are shown in table IV.

Deflections

For the five configurations studied (see table II), deflections were determined separately for airload plus inertia forces and for thermal loading. Deflections due to the elevon load were determined for configurations 1 to 4.

Figure 11 presents the wing deflections in the Z (vertical) direction due to the airloads plus inertia forces. The deflections are presented as lines of constant deflection over the wing planform. Figure 12 presents the wing deflections in the Z-direction due to the temperature distribution and figure 13 presents the wing deflections in the Z-direction due to the elevon load at the aft end of the wing tip.

Stress Resultants

Figures 14 and 15 present the inplane stress resultant (spanwise or chordwise) of largest magnitude for airloads plus inertia forces, and for thermal loading, respectively, that occur in the lower structural cover panels. Stress resultants in the lower surface were selected for presentation because the largest of them were compressive and would be of interest for structural stability considerations. Furthermore, the higher temperature levels of the lower surface make a given stress level more critical as a result of material property degradation. The maximum stress resultants in the upper cover panels were, in general, of similar magnitude to those in the lower surface but of opposite sign. The maximum tensile stresses due to the thermal loading were well below tensile yield.

Figures 14(a) to 14(e) present stress resultant contours due to airloads plus inertia forces on configurations 1 to 5. The stress in the panel caused by the maximum stress resultant contour value is shown on each of the figures presenting stress resultants and the direction of the stress resultant plotted in a figure is indicated by the arrows on the box in the figure. Figure 15 presents stress resultant contours due to thermal loading in the same order as in figure 14.

Figures 16(a) to 16(c) are sketches of the planform view of the rib and spar arrangement aft of spanwise line A-A shown in figure 15(d). The stresses indicated in figure 16 are axial thermal stresses in the upper and lower rib caps along the line A-A. Figure 16(a) presents stresses in the rib caps of configuration 4 when the rib caps are assumed to be at the same temperature as the structural cover panels. Figure 16(b) presents stresses in the rib caps of configuration 4 for temperatures determined by use of the one-dimensional heat-transfer analysis. Figure 16(c) presents temperatures in the rib caps of configuration 5 when the rib caps are assumed to be at the same temperature as the structural cover panels. The spanwise wing section selected to present rib cap stresses was chosen to be near the location of the rib cap maximum compressive stresses. Figures 17(a) to 17(d) present stress resultant contours for configurations 1 to 4 due to elevon load.

DISCUSSION OF RESULTS

Effects of Cover-Panel Concepts

The effects of the cover-panel concepts on wing deflections, temperatures, and stress resultants were obtained by comparing the results from the analyses of the three fully supported positive-camber wing configurations (configurations 1, 2, and 4).

Deflection and stress resultants due to airloads plus inertia forces.- A comparison of the wing vertical deflections for configurations 1, 2, and 4 (figs. 11(a), 11(b), and 11(d)) shows that the deflected shapes for the three configurations are similar and the deflections are small. Inasmuch as the lines of constant deflection run principally in a chordwise direction, spanwise bending is the primary cause of the vertical deflections for these configurations. The relatively small deflections exhibited by these configurations indicate that each configuration possesses adequate stiffness to support the airloads and inertial loads. The slightly larger vertical deflections exhibited by configuration 2 are a direct result of the lower total spanwise bending stiffness for this configuration.

The most significant stress resultant in the cover panels of configuration 1 and configuration 4 (figs. 14(a) and 14(d)) is the spanwise axial-stress resultant. For configuration 2, where the spar caps provide the spanwise bending stiffness, stress resultants less than 50 lbf/in. (8.8 kN/m) are developed in the cover panels. Cover-panel stresses are below the elevated-temperature yield stress of the material for all configurations.

Panel temperatures.- Comparison of the panel temperature history curves for a point on the root chord 11.6 feet (3.54 meters) aft of the leading edge on configurations 1 and 2 (figs. 6(a) and 6(b)) indicates that the average temperatures of the upper or lower surface panels are approximately the same. The average temperatures of the panels in configuration 4 (fig. 6(c)), however, are considerably less than those for the panels in configurations 1 and 2 because of the insulating effect of the aerodynamic surfaces present in configuration 4. At the design condition, however, the difference between the average temperatures of the top and bottom cover panels of the three configurations is not significantly altered by the cover-panel configuration or the presence of the aerodynamic surface.

Temperature gradients through the upper panel of configuration 2 vary considerably during the flight. This large variation in temperature gradient is caused by the reduction in aerodynamic heating on the exterior upper surface resulting from the sudden increase in angle of attack during the turn. The presence of the aerodynamic surface in configuration 4 prohibits a similar large variation in depthwise temperature gradient in the panel during the turn. In configuration 1 it was assumed that the panels were thin, and consequently, no depthwise temperature gradients existed in the panels.

The temperature distribution imposed upon the structure in the present analysis results in a more severe design condition than a comparable Mach 8 steady-state design condition. Average lower panel temperatures at the design condition and location indicated in figure 6 for configurations 1 and 2 equal the panel temperature that would be obtained at the same wing location during steady-state flight at Mach 8 and a dynamic pressure of approximately 1200 psf (57.5 kN/m^2). Temperature gradients through the depth of the wing are smaller for the steady-state flight condition. Calculations for configuration 4 indicate that the lower cover panel average steady-state temperature would be only about 50° R (28 K) less than the corresponding values in configurations 1 and 2. Thus, as would be expected, the insulating effect of the aerodynamic surface is most effective during a transient heating condition.

In the absence of thermal protection, the cover-panel temperatures near the leading edge of configurations 1 and 2 exceeded the working temperature of the structural material. In order to reduce the cover-panel temperature near the leading edge, the forward part of the wing was insulated. The effect on the temperature distribution is shown by the dashed lines in figure 7(a). For this insulation concept, it was assumed that the effective thermal conductivity of the insulation could be varied to give a smooth temperature distribution in the cover panels. The use of a single skin as a heat shield, similar to the aerodynamic surface of configuration 4, was not desirable because of the resulting discontinuities in structural temperatures and surface contour where the shielding ends. Insulation was not required in configuration 4 since the aerodynamic surface served as a heat shield.

Beam-cap temperatures.- The structural analysis for each configuration was made by assuming beam-cap temperatures equal to the temperature of the adjoining cover panel. This assumption results in the most severe depthwise temperature gradients possible in the beams of the substructure. The assumption is valid, however, if the caps are of relatively light construction, are fastened directly to the cover panels, and the primary mode of heat transfer through the cover panels at the caps is conduction.

In order to obtain another possible beam-cap temperature distribution, the beam caps were included in a thermal analysis for configuration 4 in which the tubular panel shape was assumed to be continuous across the beam caps. This construction greatly reduces heat conduction into the caps and results in significantly lower beam temperatures and depthwise temperature gradients in the beams. Thus, the cover panels and method of attachment to the substructure can significantly alter the substructure temperature distribution.

Thermal vertical deflections.- The effects of the three cover-panel concepts on thermal vertical deflections are shown in figures 12(a), 12(b), and 12(d). For these configurations the magnitudes of the deflections are small and the deflected shapes are similar. Configuration 1 exhibits the largest deflections and configuration 2, the largest amount of chordwise bending. The slightly larger deflections obtained for configuration 1 are caused by the combined action of the chordwise thermal loads in the panels and the higher Poisson's ratio for the panels of configuration 1. Using the less severe temperature distribution in the substructure of configuration 4 did not appreciably alter the deflected shape from that shown in figure 12(d).

Thermal-stress resultants.- The chordwise stress resultants N_X in the lower panels of configuration 1 due to thermal loading (fig. 15(a)) have a maximum of approximately -1400 lbf/in. (-245 kN/m) which corresponds to about four times the maximum spanwise compressive stress resultant due to airloads plus inertia forces. In comparison with the airload plus inertia force stress resultants, the high compressive thermal-stress resultants affect a much larger area of the cover panels. This condition may result in an appreciable weight penalty if panel thicknesses have to be increased in the high stress region to prevent buckling. The spanwise thermal-stress resultants N_Y for configuration 1 are less than 20 percent of N_X in the areas where N_X is large and are of approximately the same magnitude as the airload plus inertia force stress resultants.

The magnitude and pattern of the chordwise thermal-stress resultants in the panels of configuration 1 and configuration 2 are similar. (See figs. 15(a) and 15(b).) Inasmuch as the panels in configuration 1 have biaxial stiffness and the panels of configuration 2 have no significant axial stiffness in the spanwise direction, the spanwise axial stiffness properties of the panels do not significantly contribute to the large thermal-stress resultants in the panels of these configurations.

The significant thermal-stress resultants for configuration 4 are in the spanwise direction (fig. 14(d)) and are of similar magnitude to the airload plus inertia force stress resultants. For the configuration 4 case in which the cap temperatures are below the cover-panel temperatures, the stress resultant contour pattern is approximately the same as that shown in figure 14(d). However, the maximum stress resultants are approximately 10 percent lower. In both cases for configuration 4 the thermal-stress resultants are caused principally by the boundary loads along the root rib which keep the root rib from bowing in the plane of the wing. Thus, orienting the axial stiffness of the cover panels more nearly in the direction of the cover-panel temperature gradients greatly reduces the magnitude of the thermal-stress resultants in the cover panels.

Beam-cap thermal stresses.- As noted previously, the local method of attachment between the beam caps and cover panels can significantly alter the magnitude of the temperatures and temperature gradients in the substructure. The corresponding effect on cap stresses is seen in figures 16(a) and 16(b) where the cap stresses are presented for configuration 4 for the two substructure temperature distributions investigated. When the cap temperatures are equal to their respective adjacent cover-panel temperatures, the resulting thermal stress in the caps (fig. 16(a)) is high and exceeds the yield stress of the material at the leading edge in this configuration. When the cover panels provide thermal protection for the substructure, the cap stresses are significantly reduced, as indicated by the stresses shown in figure 16(b). From these results it appears that proper panel geometry and orientation (that is, panels possessing uniaxial stiffness in the spanwise direction) combined with thermal protection for the substructure that provides bending and axial stiffness in the chordwise direction results in a wing configuration with relatively low thermal loads.

Effects of Root Support

The effects of root support on wing characteristics were obtained by comparing the results for the fully supported wing of configuration 2 with the two-point supported wing of configuration 3. These configurations are identical except for the support systems and additional bending stiffness in the two spars at the support locations of configuration 3.

Deflections and stress resultants due to airloads plus inertia loads.- Examination of the wing vertical deflection contours for configuration 3 (fig. 11(c)) indicates that aft of the front-support point, the deflections are primarily caused by spanwise bending, the maximum deflection in this region occurring at the wing tip. Forward of the front support point, the wing vertical deflections are primarily caused by chordwise bending. For configuration 3 the deflections are relatively small and are of comparable magnitude to those in configuration 2. Thus, if adequate bending stiffness is provided in the two main spars at the support points (configuration 3), the two-point-supported configuration possesses adequate stiffness to support the airload plus inertia force.

The most significant stress resultant for configuration 3 is the chordwise axial-stress resultant (fig. 14(c)) caused primarily by chordwise bending. Although the magnitudes of the stress resultant have significantly increased over those present in configuration 2, they cause stresses far below the elevated-temperature yield stress of the material.

Deflections and stress resultants due to temperature distribution.- Examination of the wing vertical deflections for configuration 3 (fig. 12(c)) indicates that for the unconstrained wing, chordwise thermal bowing is large. This bowing could cause sealing problems between the wing and fuselage and significant changes in the aircraft characteristics and in the airload and temperature distributions on the wing.

Thermal-stress resultants are caused by nonlinear temperature gradients within the wing and the constraints imposed on the wing by the support structure. Thus, as would be expected, the thermal-stress resultants in configuration 3 are considerably lower than those of configuration 2. The nonlinearity of the inplane temperature distribution, however, still produces stress resultants that are several times greater than those produced by the airloads plus inertia forces. If the forward part of the wing was allowed to reach higher temperatures to attain more uniform temperature distributions in the cover panels, the stress resultants would be reduced for configuration 3. The deflections of configuration 3, however, would probably increase.

Effects of Wing Camber

The effects of camber on the design parameters may be determined by comparing the results of the analyses for configuration 4 and configuration 5. These configurations are identical except for the inverted airfoil section which changes the camber from a positive value (configuration 4) to an equal negative value (configuration 5).

Panel temperatures.- One of the most significant effects of the large change in camber is in the rearrangement of the temperature distribution. Along the root-chord line between stations 11.6 and 23.3, the local surface angles of attack are the same for both configurations and, consequently, the panel temperatures are the same. (See figs. 7(b) and 7(c).) Forward of this point, the relative changes in local angle of attack between configuration 4 and configuration 5 cause higher temperatures on the lower surface and lower temperatures on the upper surface of configuration 5. Similarly, the panels on the aft section of the wing of configuration 5 operate at lower temperatures than those of configuration 4. Thus, the change in camber results in large inplane temperature gradients in the lower surface of configuration 5. Further comparison of the figures indicates that configuration 5 experiences larger depthwise temperature gradients than configuration 4 in the forward part of the wing. Beam-cap temperatures were again assumed to be equal to the adjacent cover-panel temperatures.

Although the temperatures in the forward part of configuration 5 exceeded 2060° R (1144 K), which was assumed to be the maximum temperature capability of the superalloy, no insulation was used between the aerodynamic surface and the structure so that a comparison of temperatures, stress resultants, and deflections could be made between configuration 4 and configuration 5.

Deflections and stress resultants due to airloads plus inertia forces.- In the structural analysis of configuration 4, the airload distribution was assumed to be constant over the wing planform. In configuration 5 changes in local surface angles of attack result in higher airloads immediately behind the leading edge, and lower airloads over the aft part of the wing. The forward and slightly outward shift of the center of pressure for configuration 5 suggests that the wing deflections should increase and that the distribution and magnitudes of the stress resultants should change. However, comparison of the vertical deflections (figs. 11(d) and 11(e)) indicates insignificant changes in the magnitude of the deflections and deflected shape for these configurations. Similarly, there are no significant changes in the stress resultant distributions (figs. 11(d) and 11(e)). Apparently, the lower panel temperatures experienced by some of the cover panels of configuration 5 change the material properties of the panels sufficiently to compensate for the shift in center of pressure. Thus, for the configurations studied, camber has no significant net effect on the stress resultants in the lower cover panels and on the vertical deflections resulting from airloads plus inertia forces.

Deflections and stress resultants due to temperature distributions.- The effect of camber on the thermal vertical deflections are seen by comparing figures 12(d) and 12(e). The deflected shape of the negative camber wing shows a significant increase in spanwise bowing over the positive camber wing, although the tip deflection is still not excessive. This large increase in thermal deformation is caused by the larger depthwise thermal gradients in the wing.

The effect of camber on the thermal-stress resultants in the lower cover panels are seen by comparing figures 15(d) and 15(e). The figures indicate that the maximum thermal-stress resultants for the negative camber wing are compressive and exhibit large increases over the aft part of the wing when compared with those of configuration 4. Again the stress resultants in configuration 5 are mainly caused by the loads at the root boundary which are required to keep the root rib from bowing in the plane of the wing.

The stresses in the beam caps in configuration 5 also exhibit large increases over those of configuration 4. Therefore, the substructure would require thermal protection in order to decrease the beam-cap temperatures near the leading edge and lower the thermal stress to an acceptable level below the material yield stress.

Thus, although changing the wing camber may not significantly alter the airload plus inertia force deflections and stress resultants in the cover panels, it does significantly alter the thermal loads throughout the structure because of the relatively large change in distribution of aerodynamic heating, and consequently the temperature distribution in the structure.

Deflections and Stress Resultants Due to Elevon Load

The effect of elevon load on the vertical deflection of configurations 1, 2, and 4 may be seen in figures 13(a), 13(b), and 13(d). The magnitudes of the deflected shapes are similar and result from combined spanwise and chordwise bending.

The stress resultant patterns resulting from the elevon load are shown in figures 17(a), 17(b), and 17(d) for configurations 1, 2, and 4, respectively. The stress resultant patterns for configuration 1 and configuration 4 are similar but the maximum stress resultant value for configuration 4 is about 50 percent higher than that for configuration 1. This difference is probably due to the greater shear stiffness and chordwise axial stiffness of the waffle panels of configuration 1. The chordwise and shear stress resultants are both relatively low in configuration 2. In configuration 3 (fig. 17(c)), the two-point support system induces chordwise bending but the magnitude of the stress resultants is relatively small. The effect of elevon load on configuration 5 is similar to that for configuration 4.

Evaluation of Configurations

In the flight of a hypersonic aircraft it is probable that during a maneuver, such as the turn used in the present analysis, the maximum value of air, inertia, and thermal loads will occur nearly simultaneously. If a new maneuver is initiated suddenly, however, the structural temperature may lag the new aerodynamic environment significantly. Consequently, design conditions for a particular structural element may depend on the flight condition at a given instant and the prior flight path.

For the trajectory assumed in this study, it would appear that the critical stress condition would be either the additive stresses or the stresses due to temperature alone – whichever gives the greatest value. Thus the study indicates that configurations 1, 2, and 4 (with substructure thermal protection) could probably be developed for use in this aircraft inasmuch as the deformations are small and stresses are below the yield stress for the material. However, panel size or panel thickness ($\bar{t}$) may have to be altered to preclude compressive buckling in the lower surface. Reduction in panel size increases the total rib and spar weight whereas an increase in panel thickness increases the panel weight. Furthermore, the stresses should be examined to determine whether a satisfactory margin of safety can be obtained for the design condition. In evaluating configuration 4 with respect to configurations 1 and 2, the weight penalty of the nonload-carrying aerodynamic surface has to be considered in the evaluation. Another consideration is the effect of the low chordwise bending stiffness of the structural panels on configuration 4 on panel flutter.

The large deflections of configuration 3 would probably make it undesirable. However, if the large deflections are not objectionable, the resistance to flutter for the complete wing has to be determined. The high rib-cap thermal stresses and forward panel temperatures in configuration 5 would probably have to be reduced before it could be considered for use and then the weight penalty of the aerodynamic surface and panel flutter sensitivity as discussed for configuration 4 has to be considered.

CONCLUDING REMARKS

A thermal analysis and a deformation and stress analysis of five structural configurations for radiatively cooled discrete delta wings were performed by use of finite-element representations of the structural configurations. The design conditions for the analyses were a 4.5g Mach 8 turn at a dynamic pressure of 2200 psf (105 kN/m^2). The structural configurations studied included wing cover panels with either biaxial or uniaxial stiffness, wing supports either along the full length of the wing root or at two locations on the root chord, and airfoil sections possessing either positive or negative camber.

Results of the thermal analyses indicated that for the chosen structural material (René 41), all concepts require thermal protection near the leading edge of the wing to keep the material temperature below the assumed maximum operating temperature of the material (2060° R or 1144 K). Furthermore, inplane temperature gradients in the wing cover panels may be significantly affected by both the airfoil shape and the use of insulation on the exterior surface of the wing cover panels. The thermal analyses also indicated that the nonstructural aerodynamic surfaces used in configurations 4 and 5 act as an effective thermal insulator during transient heating conditions but have very little effect on the structural temperatures for a steady-state flight condition.

Results of the deformation and stress analyses indicated that deformations due to either airload plus inertial force, elevon load, or thermal load are not excessive for the configurations having attachments to the fuselage along the full length of the wing root.

The deformations of the configuration having supports at two locations along the root chord indicate that significant chordwise bowing occurs as a result of airloads plus inertia loads, and the temperature distribution in the structure. For this reason this configuration may not have acceptable stiffness properties.

When the material yield stress is used as a basis of comparison, the stresses due to airloads plus inertia loads and elevon loads are relatively small for all configurations. Axial thermal stresses, however, are high in the structural configurations having wing supports along the full length of the wing root. Results of the analysis indicate that chordwise axial stiffness in the cover panels causes large axial thermal stress to be developed in the cover panels. In contrast, cover panels which have only spanwise axial stiffness have lower values of thermal stress in the panels and high thermal stresses are confined to the caps in the substructure. This condition is believed to be advantageous since it may allow critical stress regions to be confined to local areas along the caps.

Changing the airfoil shape from positive to negative camber resulted in higher thermal stresses in the wing structure. These higher stresses resulted from the higher structural temperatures on the lower surface of the wing near the leading edge which caused larger inplane temperature gradients in the lower surface cover panels and larger temperature gradients through the depth of the wing near the leading edge.

Langley Research Center,
National Aeronautics and Space Administration,
Hampton, Va., November 7, 1970.

APPENDIX

CONVERSION OF U.S. CUSTOMARY UNITS TO SI UNITS

Conversion factors for the units used herein are given in the following table:

Physical quantity	U.S. Customary Unit	Conversion factor (*)	SI Unit (**)
Length	inches	0.0254	meters (m)
	feet	0.3048	meters (m)
Angle	degrees	0.01745329	radians (rad)
Stress resultant	pounds force/in.	175.1268	newtons/meter (N/m)
Stress	pounds force/in^2	6894.757	newtons/meter^2 (N/m^2)
Velocity	ft/sec	0.3048	meters/second (m/s)
Temperature	degrees Rankine	5/9	kelvins (K)
Pressure	pounds force/ft^2	47.88026	newtons/meter^2 (N/m^2)

*Multiply value given in U.S. Customary Unit by conversion factor to obtain equivalent value in SI unit.

**Prefixes to indicate multiple of units are as follows:

Prefix	Multiple
centi (c)	10^{-2}
kilo (k)	10^3
mega (M)	10^6
giga (G)	10^9

REFERENCES

1. Comm. on Metric Pract.: ASTM Metric Practice Guide. NBS Handbook 102, U.S. Dep. Com., Mar. 10, 1967.

2. Goldberg, Theodore J.; Hefner, Jerry N.; and Stone, David R.: Hypersonic Aerodynamic Characteristics of Two Delta-Wing X-15 Airplane Configurations. NASA TN D-5498, 1969.

3. Lemcoe, M. M.; and Trevino, Alex: Determination of the Effects of Elevated Temperature Materials Properties of Several High Temperature Alloys. ASD-TDR-61-529, U.S. Air Force, June 1962.

4. Van Driest, E. R.: Turbulent Boundary Layer in Compressible Fluids. J. Aeronaut. Sci., vol. 18, no. 3, Mar. 1951, pp. 145-160, 216.

5. Van Driest, E. R.: The Turbulent Boundary Layer With Variable Prandtl Number. Rept. No. AL-1914, North Am. Aviation, Inc., Apr. 2, 1954.

6. Minzner, R. A.; Champion, K. S. W.; and Pond, H. L.: The ARDC Model Atmosphere, 1959. Air Force Surv. in Geophys. No. 115 (AFCRC-TR-59-267), Air Force Cambridge Res. Center, Aug. 1959.

7. Ames Research Staff: Equations, Tables, and Charts for Compressible Flow. NACA Rep. 1135, 1953. (Supersedes NACA TN 1428.)

8. Jackson, L. Robert; Davis, John G., Jr.; and Wichorek, Gregory R.: Structural Concepts for Hydrogen-Fueled Hypersonic Airplanes. NASA TN D-3162, 1966.

9. Bertram, Mitchel H.; and Feller, William V.: A Simple Method for Determining Heat Transfer, Skin Friction, and Boundary-Layer Thickness for Hypersonic Laminar Boundary-Layer Flows in a Pressure Gradient. NASA MEMO 5-24-59L, 1959.

10. Melosh, Robert J.; Diether, Philip A.; and Brennan, Mary: Structural Analysis and Matrix Interpretive System (SAMIS) Program Report. Tech. Memo. No. 33-307, Revision 1 (Contract NAS 7-100), Jet Propulsion Lab., California Inst. Technol., Dec. 15, 1966.

TABLE I.- MATERIAL PROPERTIES OF RENÉ 41

Temperature		Tension modulus		Compression modulus		Thermal expansion coefficient		Tensile yield	
$^{\circ}R$	K	psi	GN/m^2	psi	GN/m^2	$1/^{\circ}R$	1/K	psi	MN/m^2
540	300	29.97×10^6	206.6	31.63×10^6	218.1	6.55×10^{-6}	11.79×10^{-6}	142×10^3	6.80
1060	589	28.22	194.6	29.59	204.0	7.13	12.83	125	5.99
1460	811	26.2	180.6	27.2	187.5	7.58	13.64	123	5.89
1560	867	26.1	180.0	27.0	186.2	7.69	13.84	122	5.84
1660	922	25.98	179.1	26.54	183.0	7.80	14.04	121	5.79
1760	978	22.8	157.2	25.5	175.8	8.00	14.4	116	5.55
1860	1033	19.57	134.9	22.15	154.8	8.20	14.76	98	4.69
1960	1089	18.84	129.9	14.97	103.2	8.43	15.17	81	3.87
2060	1144	17.3	119.3			8.68	15.62	57	2.73
2160	1200	16.0	110.3			8.95	16.11		

TABLE II.- SUMMARY OF STRUCTURAL CONFIGURATIONS

Configuration	Cover panel	Camber	Exterior surface (*)	Root support
1	Waffle	+	A	Full
2	Beaded chord stiffened	+	A	Full
3	Beaded chord stiffened	+	A	Two-point
4	Tubular span stiffened	+	B	Full
5	Tubular span stiffened	-	B	Full

*A denotes thermal protection on upper and lower forward cover panels.
B denotes aerodynamic surface over all cover panels.

TABLE III. - GRID-POINT COORDINATE DATA

[All coordinates are given in inches. U.S. Customary units are used in this table because the SAMIS program requires input data in this system of units.]

N_{gp}	$\bar{X}$ (*)	Y	$Z_{(1,2,3)}$ (**)	$Z_{(4,5)}$ (**)	N_{gp}	$\bar{X}$ (*)	Y	$Z_{(1,2,3)}$ (**)	$Z_{(4,5)}$ (**)
1	0.00	0.00	0.15	0.50	51	150.00	-15.29	5.63	5.28
2	.00	.00	1.73	1.38	52	150.00	-15.29	10.41	10.06
3	.00	.00	2.62	2.27	53	150.00	.00	.15	.50
4	.00	19.50	-8.80	-8.80	54	150.00	.00	6.59	6.24
5	.00	19.50	21.20	21.20	55	150.00	.00	12.33	11.98
6	30.00	-7.64	.15	.50	56	150.00	19.50	-8.80	-8.80
7	30.00	-7.64	1.68	1.33	57	150.00	19.50	21.20	21.20
8	30.00	-7.64	2.52	2.17	58	180.00	-45.87	.15	.50
9	30.00	.00	.15	.50	59	180.00	-45.87	1.42	1.07
10	30.00	.00	3.74	3.39	60	180.00	-45.87	2.00	1.65
11	30.00	.00	6.63	6.28	61	180.00	-30.58	.15	.50
12	30.00	19.50	-8.80	-8.80	62	180.00	-30.58	4.55	4.20
13	30.00	19.50	21.20	21.20	63	180.00	-30.58	8.26	7.91
14	60.00	-15.29	.15	.50	64	180.00	-15.29	.15	.50
15	60.00	-15.29	1.63	1.28	65	180.00	-15.29	5.76	5.41
16	60.00	-15.29	2.42	2.07	66	180.00	-15.29	10.68	10.33
17	60.00	.00	.15	.50	67	180.00	.00	.15	.50
18	60.00	.00	5.21	4.86	68	180.00	.00	6.59	6.24
19	60.00	.00	9.57	9.22	69	180.00	.00	12.33	11.98
20	60.00	19.50	-8.80	-8.80	70	180.00	19.50	-8.80	-8.80
21	60.00	19.50	21.20	21.20	71	180.00	19.50	21.20	21.20
22	90.00	-22.93	.15	.50	72	210.00	-53.52	.15	.50
23	90.00	-22.93	1.58	1.23	73	210.00	-53.52	1.37	1.02
24	90.00	-22.93	2.31	1.96	74	210.00	-53.52	1.90	1.55
25	90.00	-15.29	.15	.50	75	210.00	-45.87	.15	.50
26	90.00	-15.29	3.59	3.24	76	210.00	-45.87	3.21	2.86
27	90.00	-15.29	6.33	5.98	77	210.00	-45.87	5.58	5.23
28	90.00	.00	.15	.50	78	210.00	-30.58	.15	.50
29	90.00	.00	6.15	5.80	79	210.00	-30.58	4.94	4.59
30	90.00	.00	11.45	11.10	80	210.00	-30.58	9.03	8.68
31	90.00	19.50	-8.80	-8.80	81	210.00	-15.29	.15	.50
32	90.00	19.50	21.20	21.20	82	210.00	-15.29	5.76	5.41
33	120.00	-30.58	.15	.50	83	210.00	-15.29	10.68	10.33
34	120.00	-30.58	1.53	1.18	84	210.00	.00	.15	.50
35	120.00	-30.58	2.21	1.86	85	210.00	.00	6.59	6.24
36	120.00	-15.29	.15	.50	86	210.00	.00	12.68	12.33
37	120.00	-15.29	4.92	4.57	87	210.00	19.50	-8.80	-8.80
38	120.00	-15.29	8.99	8.64	88	210.00	19.50	21.20	21.20
39	120.00	.00	.15	.50	89	240.00	-61.16	.15	.50
40	120.00	.00	6.56	6.21	90	240.00	-61.16	1.32	.97
41	120.00	.00	12.28	11.93	91	240.00	-61.16	1.79	1.44
42	120.00	19.50	-8.80	-8.80	92	240.00	-45.87	.15	.50
43	120.00	19.50	21.20	21.20	93	240.00	-45.87	4.04	3.69
44	150.00	-38.22	.15	.50	94	240.00	-45.87	7.24	6.89
45	150.00	-38.22	1.47	1.12	95	240.00	-30.58	.15	.50
46	150.00	-38.22	2.10	1.75	96	240.00	-30.58	4.94	4.59
47	150.00	-30.58	.15	.50	97	240.00	-30.58	9.03	8.68
48	150.00	-30.58	3.42	3.07	98	240.00	-15.29	.15	.50
49	150.00	-30.58	5.99	5.64	99	240.00	-15.29	5.76	5.41
50	150.00	-15.29	.15	.50	100	240.00	-15.29	10.68	10.33

*$\bar{X} = X - 10.33$ where X is shown in sketch on page 4.

**Subscripts denote applicable configurations.

TABLE III.- GRID-POINT COORDINATE DATA – Concluded

N_{gp}	$\bar{X}$ (**)	Y	$Z_{(1,2,3)}$ (**)	$Z_{(4,5)}$ (**)	N_{gp} (*)	$\bar{X}$	Y	$Z_{(1,2,3)}$ (**)	$Z_{(4,5)}$ (**)
101	240.00	0.00	0.15	0.50	141	300.00	0.00	0.15	0.50
102	240.00	.00	6.59	6.24	142	300.00	.00	6.31	5.96
103	240.00	.00	12.33	11.98	143	300.00	.00	11.78	11.43
104	240.00	19.50	-8.80	-8.80	144	300.00	19.50	-8.80	-8.80
105	240.00	19.50	21.20	21.20	145	300.00	19.50	21.20	21.20
106	270.00	-68.81	.15	.50	146	330.00	-78.13	.15	.50
107	270.00	-68.81	1.26	.91	147	330.00	-78.13	2.30	1.95
108	270.00	-68.81	1.68	1.33	148	330.00	-78.13	3.75	3.40
109	270.00	-61.16	.15	.50	149	330.00	-61.16	.15	.50
110	270.00	-61.16	2.93	2.58	150	330.00	-61.16	3.29	2.94
111	270.00	-61.16	5.02	4.67	151	330.00	-61.16	5.74	5.39
112	270.00	-45.87	.15	.50	152	330.00	-45.87	.15	.50
113	270.00	-45.87	4.12	3.77	153	330.00	-45.87	4.12	3.77
114	270.00	-45.87	7.39	7.04	154	330.00	-45.87	7.39	7.04
115	270.00	-30.58	.15	.50	155	330.00	-30.58	.15	.50
116	270.00	-30.58	4.94	4.59	156	330.00	-30.58	4.77	4.42
117	270.00	-30.58	9.03	8.68	157	330.00	-30.58	8.70	8.35
118	270.00	-15.29	.15	.50	158	330.00	-15.29	.15	.50
119	270.00	-15.29	5.76	5.41	159	330.00	-15.29	5.22	4.87
120	270.00	-15.29	10.68	10.33	160	330.00	-15.29	9.60	9.25
121	270.00	.00	.15	.50	161	330.00	.00	.15	.50
122	270.00	.00	6.58	6.23	162	330.00	.00	5.56	5.21
123	270.00	.00	12.32	11.97	163	330.00	.00	10.27	9.92
124	270.00	19.50	-8.80	-8.80	164	330.00	19.50	-8.80	-8.80
125	270.00	19.50	21.20	21.20	165	330.00	19.50	21.20	21.20
126	300.00	-76.45	.15	.50	166	355.30	-78.13	.15	.50
127	300.00	-76.45	1.21	.86	167	355.30	-78.13	2.38	2.03
128	300.00	-76.45	1.58	1.23	168	355.30	-78.13	3.91	3.56
129	300.00	-61.16	.15	.50	169	354.00	-61.16	.15	.50
130	300.00	-61.16	3.29	2.94	170	354.00	-61.16	3.28	2.93
131	300.00	-61.16	5.74	5.39	171	354.00	-61.16	5.72	5.37
132	300.00	-45.87	.15	.50	172	352.80	-45.87	.15	.50
133	300.00	-45.87	4.12	3.77	173	352.80	-45.87	3.86	3.51
134	300.00	-45.87	7.39	7.04	174	352.80	-45.87	6.87	6.52
135	300.00	-30.58	.15	.50	175	351.50	-30.58	.15	.50
136	300.00	-30.58	4.94	4.59	176	351.50	-30.58	4.25	3.90
137	300.00	-30.58	9.03	8.68	177	351.50	-30.58	7.66	7.31
138	300.00	-15.29	.15	.50	178	350.30	-15.29	.15	.50
139	300.00	-15.29	5.72	5.37	179	350.30	-15.29	4.56	4.21
140	300.00	-15.29	10.60	10.25	180	350.30	-15.29	8.28	7.93
					181	349.10	.00	.15	.50
					182	349.10	.00	4.83	4.48
					183	349.10	.00	8.81	8.46
					184	349.10	19.50	-8.80	-8.80
					185	349.10	19.50	21.20	21.20

* $\bar{X} = X - 10.33$ where X is shown in sketch on page 4.

** Subscripts denote applicable configurations.

TABLE IV.- BEAM ELEMENT PROPERTIES

[U.S. Customary units are used in this table because the SAMIS program requires input data in this system of units. All other beam elements are identical to those for configuration 2 except that the $A_x = 0.00001$ and $I_y = 0.0000$.]

(a) Configuration 1

N	$N_{gp,1}$	$N_{gp,2}$	A_x, in^2	A_z, in^2	I_y, in^4	T_m, °R
5	2	5	0.240	0.032	0.245	800
6	1	4	.120	.00001	.00001	800
8	10	13	.240	.094	1.635	800
9	9	12	.120	.00001	.00001	800
17	18	21	.240	.146	3.93	800
18	17	20	.120	.00001	.00001	800
30	29	32	.240	.182	6.130	800
31	28	31	.120	.00001	.00001	800
45	40	43	.240	.199	7.320	800
46	39	42	.120	.00001	.00001	800
64	54	57	.240	.199	7.350	800
65	53	56	.120	.00001	.00001	800
85	68	71	.330	.199	10.11	800
86	67	70	.210	.00001	.00001	800
110	85	88	.330	.199	10.10	800
111	84	87	.220	.00001	.00001	800
133	105	86	.300	.00001	.00001	800
138	102	105	.435	.199	13.22	800
139	101	104	.290	.00001	.00001	800
169	122	125	.525	.199	16.09	800
170	121	124	.350	.00001	.00001	800
202	142	145	.675	.189	18.52	800
203	141	144	.450	.00001	.00001	800
235	162	165	.750	.159	14.62	800
236	161	164	.500	.00001	.00001	800
268	182	185	.870	.132	11.62	800
269	181	184	.580	.00001	.00001	800

TABLE IV.- BEAM ELEMENT PROPERTIES – Continued

(b) Configuration 2

N	$N_{gp,1}$	$N_{gp,2}$	A_x, in^2	A_z, in^2	I_y, in^4	T_m, °R	T_z, °R/in.	N	$N_{gp,1}$	$N_{gp,2}$	A_x, in^2	A_z, in^2	I_y, in^4	T_m, °R	T_z, °R/in.
1	2	7	0.120	0.043	0.176	1550		134	90	93	0.120	0.039	0.570	1638	-63.07
4	10	2	.00001	.043	.00001	1570	-20.31	135	93	96	.120	.072	1.910	1725	-56.39
5	2	5	.240	.032	.245	800		136	96	99	.190	.087	4.470	1810	-21.3
6	1	4	.120	.00001	.00001	800		137	99	102	.290	.102	9.360	1785	-27.5
7	7	10	.120	.039	.576	1568	-19.86	138	102	105	.435	.199	13.22	800	
8	10	13	.240	.094	1.635	800		139	101	104	.290	.00001	.00001	800	
9	9	12	.120	.00001	.00001	800		140	90	107	.120	.029	.076	1550	
10	7	15	.120	.042	.162	1550		143	110	90	.00001	.029	.00001	1605	-70.55
15	18	10	.00001	.072	.00001	1588	-23.65	148	113	93	.00001	.065	.00001	1768	-63.46
16	15	18	.120	.048	.0859	1580	-30.65	153	116	96	.00001	.080	.00001	1697	
18	17	20	.120	.00001	.00001	800		158	119	99	.00001	.095	.00001	1675	
19	15	23	.120	.040	.148	1550		163	122	102	.00001	.110	.00001	1657	
22	26	15	.00001	.038	.00001	1572	-25.06	164	107	110	.120	.029	.307	1608	-73.44
27	29	18	.00001	.102	.00001	1641	-24.82	165	110	113	.120	.054	1.100	1740	-72.73
28	23	26	.120	.038	.522	1571	-25.90	166	113	116	.140	.073	2.270	1723	-53.97
29	26	29	.120	.079	2.290	1631	-30.89	167	116	119	.240	.087	5.650	1810	-27.1
30	29	32	.240	.182	6.130	800		168	119	122	.350	.102	11.27	1785	-28.5
31	28	31	.120	.00001	.00001	800		169	122	125	.525	.199	16.09	800	
32	23	34	.120	.038	.134	1550		170	121	124	.350	.00001	.00001	800	
37	37	26	.00001	.068	.00001	1608	-31.29	171	107	127	.120	.027	.066	1550	
42	40	29	.00001	.106	.00001	1720	-29.01	176	130	110	.00001	.047	.00001	1715	-78.39
43	34	37	.120	.048	.859	1590	-35.33	181	133	113	.00001	.065	.00001	1733	-60.08
44	37	40	.120	.093	3.230	1710	-31.79	186	136	116	.00001	.080	.00001	1687	
45	40	43	.240	.199	7.320	800		191	139	119	.00001	.094	.00001	1665	
46	39	42	.120	.00001	.00001	800		196	142	122	.00001	.107	.00001	1635	
47	34	45	.120	.036	.121	1550		197	127	130	.120	.032	.370	1717	-104.27
50	48	34	.00001	.036	.00001	1571	-35.95	198	130	133	.130	.058	1.336	1753	-55.21
55	51	37	.00001	.086	.00001	1694	-34.35	199	133	136	.220	.073	3.580	1820	-24.0
60	54	40	.00001	.109	.00001	1707		200	136	139	.340	.087	7.940	1790	-30.6
61	45	48	.120	.035	.453	1580	-28.00	201	139	142	.450	.098	13.72	1780	-34.2
62	48	51	.120	.073	1.952	1656	-35.78	202	142	145	.675	.189	18.52	800	
63	51	54	.120	.101	3.780	1715	-38.32	203	141	144	.450	.00001	.00001	800	
64	54	57	.240	.199	7.350	800		204	127	147	.120	.045	.190	1550	
65	53	56	.120	.00001	.00001	800		209	150	130	.00001	.050	.00001	1768	-81.40
66	45	59	.120	.034	.108	1550		214	153	133	.00001	.065	.00001	1697	
71	62	48	.00001	.063	.00001	1632	-38.54	219	156	136	.00001	.079	.00001	1675	
76	65	51	.00001	.094	.00001	1717	-40.10	224	159	139	.00001	.090	.00001	1610	
81	68	54	.00001	.110	.00001	1687		229	162	142	.00001	.098	.00001	1587	
82	59	62	.120	.045	.744	1608	-46.99	230	147	150	.120	.042	.663	1793	-103.19
83	62	65	.120	.084	2.610	1718	-42.38	231	150	153	.120	.058	1.234	1723	-67.86
84	65	68	.210	.102	6.760	1810	-16.8	232	153	156	.230	.071	3.590	1805	-34.9
85	68	71	.330	.199	10.11	800		233	156	159	.360	.081	7.290	1785	-39.5
86	67	70	.210	.00001	.00001	800		234	159	162	.500	.088	11.96	1765	-47.2
87	59	73	.120	.032	.097	1550		235	162	165	.750	.159	14.62	800	
90	76	59	.00001	.032	.00001	1580		236	161	164	.500	.00001	.00001	800	
95	79	62	.00001	.077	.00001	1717	-43.06	237	147	167	.00001	.066	.00001	1820	-141.30
100	82	65	.00001	.095	.00001	1717		242	170	150	.00001	.050	.00001	1740	-78.85
105	85	68	.00001	.110	.00001	1675		247	173	153	.00001	.063	.00001	1680	
106	73	76	.120	.032	.387	1580	-29.8	252	176	156	.00001	.072	.00001	1655	
107	76	79	.120	.064	1.532	1713	-45.45	257	179	159	.00001	.079	.00001	1605	
108	79	82	.120	.087	2.820	1720	-45.36	262	182	162	.00001	.169	.00001	1750	-56.7
109	82	85	.220	.102	7.090	1810	-23.1	263	167	170	.120	.042	.650	1759	-97.21
110	85	88	.330	.199	10.10	800		264	170	173	.130	.055	1.230	1790	-34.0
111	84	87	.220	.00001	.00001	800		265	173	176	.270	.064	3.410	1780	-42.4
112	73	90	.120	.031	.087	1550		266	176	179	.430	.070	6.570	1800	-54.5
117	93	76	.00001	.056	.00001	1688	-51.92	267	179	182	.580	.076	10.23	1750	-59.3
122	96	79	.00001	.080	.00001	1725	-50.68	268	182	185	.870	.132	11.62	800	
127	99	82	.00001	.095	.00001	1685		269	181	184	.580	.00001	.00001	800	
132	102	85	.00001	.110	.00001	1667									
133	105	86	.300	.00001	.00001	800									

TABLE IV.- BEAM ELEMENT PROPERTIES – Continued

(c) Configuration 3

N	$N_{gp,1}$	$N_{gp,2}$	A_x, in^2	A_z, in^2	I_y, in^4	T_m, ^oR	T_z, ^oR/in.
1	2	7	0.120	0.043	0.176	1550	
4	10	2	.00001	.043	.00001	1570	-20.31
5	7	10	.120	.039	.576	1568	-19.86
6	7	15	.120	.042	.162	1550	
11	18	10	.00001	.072	.00001	1588	-23.65
12	15	18	.120	.048	.859	1580	-30.65
13	15	23	.120	.040	.148	1550	
16	26	15	.00001	.038	.00001	1572	-25.06
21	29	18	.00001	.102	.00001	1641	-24.82
22	23	26	.120	.038	.522	1571	-25.90
23	26	29	.120	.079	2.290	1631	-30.89
24	23	34	.120	.038	.134	1550	
29	37	26	.00001	.068	.00001	1608	-31.29
34	40	29	.00001	.106	.00001	1720	-29.01
35	34	37	.120	.048	.859	1590	-35.33
36	37	40	.120	.093	3.230	1710	-31.79
37	34	45	.120	.036	.121	1550	
40	48	34	.00001	.036	.00001	1571	-35.95
45	51	37	.00001	.086	.00001	1694	-34.35
50	54	40	.00001	.109	.00001	1707	
51	45	48	.360	.105	1.359	1580	-27.5
52	48	51	.360	.216	5.856	1656	-35.78
53	51	54	.360	.303	11.340	1715	-38.32
54	54	57	.720	.600	21.150	800	
55	53	56	.360	.00030	.00003	800	
56	45	59	.120	.034	.108	1550	
61	62	48	.00001	.063	.00001	1632	-38.54
66	65	51	.00001	.094	.00001	1717	-40.10
71	68	54	.00001	.110	.00001	1687	
72	59	62	.120	.045	.744	1608	-46.99
73	62	65	.120	.084	2.610	1718	-42.38
74	65	68	.210	.102	6.760	1810	-16.8
75	59	73	.120	.032	.097	1550	
78	76	59	.00001	.032	.00001	1580	
83	79	62	.00001	.077	.00001	1717	-43.06
88	82	65	.00001	.095	.00001	1707	
93	85	68	.00001	.110	.00001	1675	
94	73	76	.120	.032	.387	1580	-29.8
95	76	79	.120	.064	1.532	1713	-45.45
96	79	82	.120	.087	2.820	1720	-45.36
97	82	85	.220	.102	7.090	1910	-23.1
98	73	90	.120	.031	.087	1550	
103	93	76	.00001	.056	.00001	1688	-51.92
108	96	79	.00001	.080	.00001	1725	-50.68
113	99	82	.00001	.095	.00001	1685	
118	102	85	.00001	.110	.00001	1667	
119	90	93	.120	.039	.570	1638	-63.07
120	93	96	.120	.072	1.910	1725	-56.39
121	96	99	.190	.087	4.470	1810	-21.3
122	99	102	.290	.102	9.360	1785	-27.5

N	$N_{gp,1}$	$N_{gp,2}$	A_x, in^2	A_z, in^2	I_y, in^4	T_m, ^oR	T_z, ^oR/in.
123	90	107	0.120	0.029	0.076	1550	
126	110	90	.00001	.029	.00001	1605	-70.55
131	113	93	.00001	.065	.00001	1768	-63.46
136	116	96	.00001	.080	.00001	1697	
141	119	99	.00001	.095	.00001	1675	
146	122	102	.00001	.110	.00001	1657	
147	107	110	.120	.029	.307	1608	-73.44
148	110	113	.120	.054	1.100	1740	-72.73
149	113	116	.140	.073	2.270	1723	-53.97
150	116	119	.240	.087	5.650	1810	-27.1
151	119	122	.350	.102	11.27	1785	-28.5
152	107	127	.120	.027	.066	1550	
157	130	110	.00001	.047	.00001	1715	-78.39
162	133	113	.00001	.065	.00001	1733	-60.08
167	136	116	.00001	.080	.00001	1687	
172	139	119	.00001	.094	.00001	1665	
177	142	122	.00001	.107	.00001	1635	
178	127	130	.720	.096	1.110	1717	-104.27
179	130	133	.780	.348	8.000	1753	-55.21
180	133	136	1.320	.426	10.000	1820	-24.0
181	136	139	2.040	.500	48.000	1790	-30.6
182	139	142	2.700	.600	180.00	1780	-34.2
183	142	145	4.000	.999	111.0	800	
184	141	144	2.700	.00030	.00003	800	
185	127	147	.120	.045	.190	1550	
190	150	130	.00001	.050	.00001	1768	-81.40
195	153	133	.00001	.065	.00001	1697	
200	156	136	.00001	.079	.00001	1675	
205	159	139	.00001	.090	.00001	1610	
210	162	142	.00001	.098	.00001	1587	
211	147	150	.120	.042	.663	1793	-103.19
212	150	153	.120	.058	1.234	1723	-67.86
213	153	156	.230	.071	3.590	1805	-34.9
214	156	159	.360	.081	7.290	1785	-39.5
215	159	162	.500	.088	11.96	1765	-47.2
216	147	167	.00001	.066	.00001	1820	-141.30
221	170	150	.00001	.050	.00001	1740	-78.85
226	173	153	.00001	.063	.00001	1680	
231	176	156	.00001	.072	.00001	1655	
236	179	159	.00001	.079	.00001	1605	
241	182	162	.00001	.169	.00001	1750	-56.7
242	167	170	.120	.042	.650	1759	-97.21
243	170	173	.130	.055	1.230	1790	-34.0
244	173	176	.270	.064	3.410	1780	-42.4
245	176	179	.430	.070	6.570	1800	-54.5
246	179	182	.580	.076	10.23	1750	-59.3

TABLE IV.- BEAM ELEMENT PROPERTIES – Continued

(d) Configurations 4 and 5

N	$N_{gp,1}$	$N_{gp,2}$	A_x, in^2	A_z, in^2	I_y, in^4	Configuration 4 (*)				Configuration 5	
						A		B			
						T_m, ^oR	T_z, ^oR/in.	T_m, ^oR	T_z, ^oR/in.	T_m, ^oR	T_z, ^oR/in.
1	2	7	0.120	0.043	0.176	1300		1930	-81.4	1928	-41.0
4	10	2	.120	.043	.364	1225	-11.2	1800	-52.9	1845	-182.5
5	2	5	.240	.032	.245	800		800		800	
6	1	4	.120	.00001	.00001	800		800		800	
7	7	10	.00001	.039	.00001	1225		1812	-50.3	1990	-163.0
8	10	13	.240	.094	1.635	800		800		800	
9	9	12	.120	.00001	.00001	800		800		800	
10	7	15	.120	.042	.162	1300		1930	-86.4	1928	-435.2
15	18	10	.120	.072	1.450	1105	-11.3	1658	-31.0	1715	-86.9
16	15	18	.00001	.048	.00001	1140		1758	-44.1	1775	-146.2
17	18	21	.240	.146	3.93	800		800		800	
18	17	20	.120	.00001	.00001	800		800		800	
19	15	23	.120	.040	.148	1300		1930	-92.1	1928	-463.8
22	26	15	.120	.038	.313	1225	-11.8	1818	-49.6	1820	-187.0
27	29	18	.120	.102	3.220	1035	-9.7	1545	-27.2	1598	-53.0
28	23	26	.00001	.038	.00001	1225		1818	-50.4	1838	-191.6
29	26	29	.00001	.079	.00001	1050		1600	-32.3	1670	-77.1
30	29	32	.240	.182	6.130	800		800		800	
31	28	31	.120	.00001	.00001	800		800		800	
32	23	34	.120	.038	.134	1300		1930	-99.3	1928	-500.0
37	37	26	.120	.068	1.271	1100	-13.3	1628	-37.4	1695	-89.6
42	40	29	.120	.106	3.450	990	-15.4	1465	-31.8	1488	-43.1
43	34	37	.00001	.048	.00001	1150		1750	-47.3	1772	-134.4
44	37	40	.00001	.093	.00001	1000		1495	-36.2	1532	-52.2
45	40	43	.240	.199	7.320	800		800		800	
46	39	42	.120	.00001	.00001	800		800		800	
47	34	45	.120	.036	.121	1300		1930	-106.9	1928	-538.2
50	48	34	.120	.036	.261	1240	-19.0	1805	-61.5	1828	-207.7
55	51	37	.120	.086	2.190	1020	-14.6	1520	-38.4	1552	-59.3
60	54	40	.120	.109	3.730	940	-15.2	1408	-36.2	1418	-38.0
61	45	48	.00001	.035	.00001	1225		1805	-60.8	1830	-203.7
62	48	51	.00001	.073	.00001	1050		1560	-38.1	1632	-81.0
63	51	54	.00001	.101	.00001	960		1435	-37.1	1460	-45.6
64	54	57	.240	.199	7.350	800		800		800	
65	53	56	.120	.00001	.00001	800		800		800	
66	45	59	.120	.034	.108	1300		1930	-116.7	1928	-587.5
71	62	48	.120	.063	1.074	1100	-14.3	1603	-48.6	1628	-85.2
76	65	51	.120	.094	2.647	985	-16.4	1448	-39.7	1442	-44.9
81	68	54	.120	.110	3.750	935	-15.6	1392	-37.0	1395	-36.6
82	59	62	.00001	.045	.00001	1145		1730	-58.4	1722	-134.4
83	62	65	.00001	.084	.00001	1000		1472	-45.8	1472	-53.9
84	65	68	.00001	.102	.00001	940		1402	-39.9	1400	-40.4
85	68	71	.330	.199	10.11	800		800		800	
86	67	70	.210	.00001	.00001	800		800		800	
87	59	73	.120	.032	.097	1300		1930	-127.3	1928	-640.9
90	76	59	.120	.032	.209	1225	-13.7	1792	-76.5	1812	-222.8
95	79	62	.120	.077	1.688	1025	-12.9	1495	-50.0	1508	-59.6
100	82	65	.120	.095	2.825	950	-17.1	1380	-48.8	1402	-43.2
105	85	68	.120	.110	3.750	935	-15.5	1378	-37.9	1382	-36.2
106	73	76	.00001	.032	.00001	1325		1792	-77.9	1812	-226.6
107	76	79	.00001	.064	.00001	1050		1510	-62.0	1545	-79.1
108	79	82	.00001	.087	.00001	960		1425	-45.6	1432	-50.6
109	82	85	.00001	.102	.00001	935		1385	-40.4	1395	-38.5
110	85	88	.330	.199	10.10	800		800		800	
111	84	87	.220	.00001	.00001	800		800		800	
112	73	90	.120	.031	.087	1300		1930	-140.0	1928	-70.5
117	93	76	.120	.056	.930	1100	-16.0	1575	-64.8	1592	-101.6
122	96	79	.120	.080	1.863	985	-19.2	1440	-48.9	1430	-51.3
127	99	82	.120	.095	2.825	935	-18.1	1390	-43.7	1395	-42.7
132	102	85	.120	.110	3.750	930	-16.4	1368	-37.0	1370	-37.5

*A denotes temperatures with thermal protection for beam caps.

B denotes temperatures with beam caps equal to temperature of adjacent panel temperature.

TABLE IV.- BEAM ELEMENT PROPERTIES – Concluded

(d) Configurations 4 and 5 – Concluded

N	$N_{gp,1}$	$N_{gp,2}$	A_x, in^2	A_z, in^2	I_y, in^4	Configuration 4 (*) A T_m, °R	Configuration 4 (*) A T_z, °R/in.	Configuration 4 (*) B T_m, °R	Configuration 4 (*) B T_z, °R/in.	Configuration 5 T_m, °R	Configuration 5 T_z, °R/in.
133	105	86	0.300	0.00001	0.00001	800		800		1430	
134	90	93	.00001	.039	.00001	1150		1712	-77.9	800	
135	93	96	.00001	.072	.00001	990		1452	-55.6	1452	-59.8
136	96	99	.00001	.087	.00001	935		1400	-48.9	1405	-46.7
137	99	102	.00001	.102	.00001	930		1370	-39.4	1378	-39.9
138	102	105	.435	.199	13.22	800		800		800	
139	101	104	.290	.00001	.00001	800		800		800	
140	90	107	.120	.029	.076	1300		1930	-157.3	1928	-792.1
143	110	90	.120	.029	.154	1225	-15.3	1752	-119.1	1812	-255.9
148	113	93	.120	.065	1.141	1015	-18.2	1478	-62.6	1470	-64.9
153	116	96	.120	.080	1.863	1045	-21.4	1402	-52.0	1405	-51.3
158	119	99	.120	.095	2.825	935	-18.0	1378	-44.3	1380	-42.7
163	122	102	.120	.110	3.750	925	-17.2	1355	-38.3	1362	-37.9
164	107	110	.00001	.029	.00001	1225		1768	-110.0	1798	-254.0
165	110	113	.00001	.054	.00001	1050		1495	-80.4	1518	-90.7
166	113	116	.00001	.073	.00001	960		1425	-55.7	1428	-57.7
167	116	119	.00001	.087	.00001	935		1385	-47.8	1390	-46.7
168	119	122	.00001	.102	.00001	930		1365	-41.3	1365	-41.3
169	122	125	.525	.199	16.09	800		800		800	
170	121	124	.350	.00001	.00001	800		800		800	
171	107	127	.120	.027	.066	1300		1930	-179.5	1928	-903.9
176	130	110	.120	.047	.537	1100	-19.1	1558	-87.2	1570	-119.2
181	133	113	.120	.065	1.169	990	-24.1	1430	-64.2	1432	-65.0
186	136	116	.120	.080	1.863	935	-24.1	1390	-52.6	1395	-51.3
191	139	119	.120	.094	2.700	930	-19.0	1370	-43.9	1372	-44.4
196	142	122	.120	.107	3.562	915	-19.5	1338	-40.6	1330	-39.3
197	127	130	.00001	.032	.00001	1125		1705	-106.8	1678	-222.4
198	130	133	.00001	.058	.00001	1000		1455	-71.8	1445	-75.3
199	133	136	.00001	.073	.00001	935		1405	-58.4	1402	-57.7
200	136	139	.00001	.087	.00001	930		1375	-48.0	1375	-48.0
201	139	142	.00001	.098	.00001	925		1335	-45.5	1350	-40.6
202	142	145	.675	.189	18.52	800		800		800	
203	141	144	.450	.00001	.00001	800		800		800	
204	127	147	.120	.045	.190	1225	-20.0	1740	-175.8	1725	-318.7
209	150	130	.120	.050	.633	1020	-25.0	1463	-87.9	1468	-93.1
214	153	133	.120	.065	1.169	950	-24.8	1402	-68.0	1405	-64.2
219	156	136	.120	.079	1.789	935	-21.8	1372	-55.5	1382	-51.8
224	159	139	.120	.090	2.400	930	-20.6	1332	-52.4	1358	-46.0
229	162	142	.120	.098	2.930	900	-20.7	1302	-47.6	1268	-44.7
230	147	150	.00001	.042	.00001	1050		1510	-120.0	1515	-100.0
231	150	153	.00001	.058	.00001	960		1422	-70.9	1412	-74.4
232	153	156	.00001	.071	.00001	935		1380	-61.1	1388	-57.6
233	156	159	.00001	.081	.00001	930		1337	-59.6	1362	-52.4
234	159	162	.00001	.088	.00001	910		1302	-55.6	1320	-48.5
235	162	165	.750	.159	14.62	800		800		800	
236	161	164	.500	.00001	.00001	800		800		800	
237	147	167	.120	.066	.406	1125	-13.6	1520	-181.2	1512	-152.7
242	170	150	.120	.050	.629	900	-31.4	1435	-84.0	1428	-87.1
247	173	153	.120	.063	1.074	935	-28.0	1378	-72.5	1392	-66.1
252	176	156	.120	.072	1.481	930	-24.2	1332	-68.9	1370	-58.7
257	179	159	.120	.079	1.820	910	-24.4	1305	-64.3	1330	-53.2
262	182	162	.120	.169	2.640	890	-25.0	1278	-59.3	1175	-56.4
263	167	170	.00001	.042	.00001	990		1448	-114.9	1445	-108.6
264	170	173	.00001	.055	.00001	960		1382	-85.3	1400	-75.2
265	173	176	.00001	.064	.00001	935		1338	-80.3	1375	-65.5
266	176	179	.00001	.070	.00001	925		1310	-74.4	1350	-59.0
267	179	182	.00001	.076	.00001	890		1282	-68.2	1238	-61.7
268	182	185	.870	.132	11.62	800		800		800	
269	181	184	.580	.00001	.00001	800		800		800	

*A denotes temperatures with thermal protection for beam caps.

B denotes temperatures with beam caps equal to temperature of adjacent panel temperature.

TABLE V.- PLATE ELEMENT INPUT DATA

Configuration	D_{11}/E	D_{21}/E	D_{22}/E	D_{33}/E	D_{41}/E	D_{42}/E	D_{44}/E	D_{55}/E	D_{66}/E
1	0.697	0.317	0.697	0.317	0	0	0.519	0.1184	0.1184
2, 3	1.00	.0001	.0001	.286	0	0	.0001	.0001	.0001
4	.0001	.0001	1.000	.286	0	0	.0001	.0001	.0001
5	1.00	0	.001243	.2637	0	2.661×10^{-5}	6.739×10^{-7}	.2308	.3852

The D_{ij} are the stiffness coefficients relating stress and strain by

$$\begin{Bmatrix} \sigma_{xx} \\ \sigma_{yy} \\ \sigma_{xy} \\ \sigma_{zz} \\ \sigma_{xz} \\ \sigma_{yz} \end{Bmatrix} = \begin{bmatrix} D_{11} & & & \text{Symmetrical} & & \\ D_{21} & D_{22} & & & & \\ 0 & 0 & D_{33} & & & \\ D_{41} & D_{42} & 0 & D_{44} & & \\ 0 & 0 & 0 & 0 & D_{55} & \\ 0 & 0 & 0 & 0 & 0 & D_{66} \end{bmatrix} \begin{Bmatrix} \epsilon_{xx} \\ \epsilon_{yy} \\ \epsilon_{xy} \\ \epsilon_{zz} \\ \epsilon_{xz} \\ \epsilon_{yz} \end{Bmatrix}$$

TABLE VI.- BOUNDARY CONDITIONS AT WING-FUSELAGE ATTACHMENTS

Configuration (Table II)	N_{gp}	δ_X	δ_Y	δ_Z	θ_X	θ_Y	θ_Z
1, 2, 4, 5	4, 12, 20, 31, 42, 56, 70, 87, 104, 124, 144, 164, 184	0	0	0			
	5, 13, 21, 32, 43, 57, 71, 88, 105, 125, 145, 165, 185	0	0	0		0	0
3	54	0					
	56, 144	0	0	0			
	57, 145	0	0	0		0	0

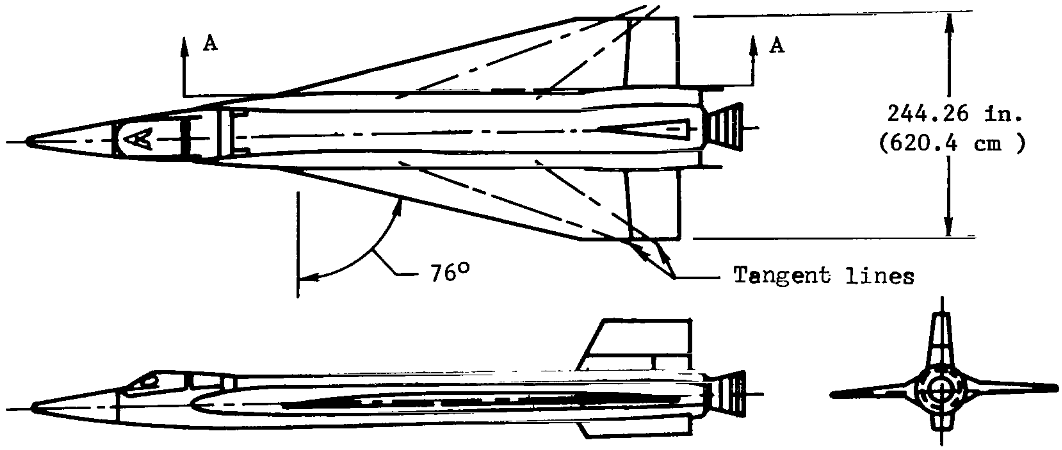

Wing area = 491.3 ft^2 (45.64 m^2)

Elevon area = 60.9 ft^2 (5.66 m^2)

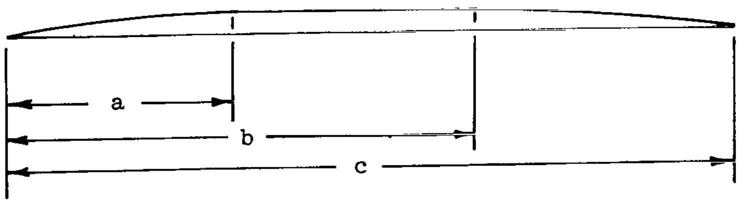

Chord length			Wing depth	
Dimension	in.	cm	in.	cm
a	133.02	377.87	12.48	31.70
b	272.24	691.49	12.48	31.70
c	417.65	1060.84	2.04	5.18

Section A–A – Root chord 44.0 in. (111.76 cm) from vehicle center line
Leading-edge radius = 0.75 in. (1.91 cm)

Figure 1.- Vehicle geometry.

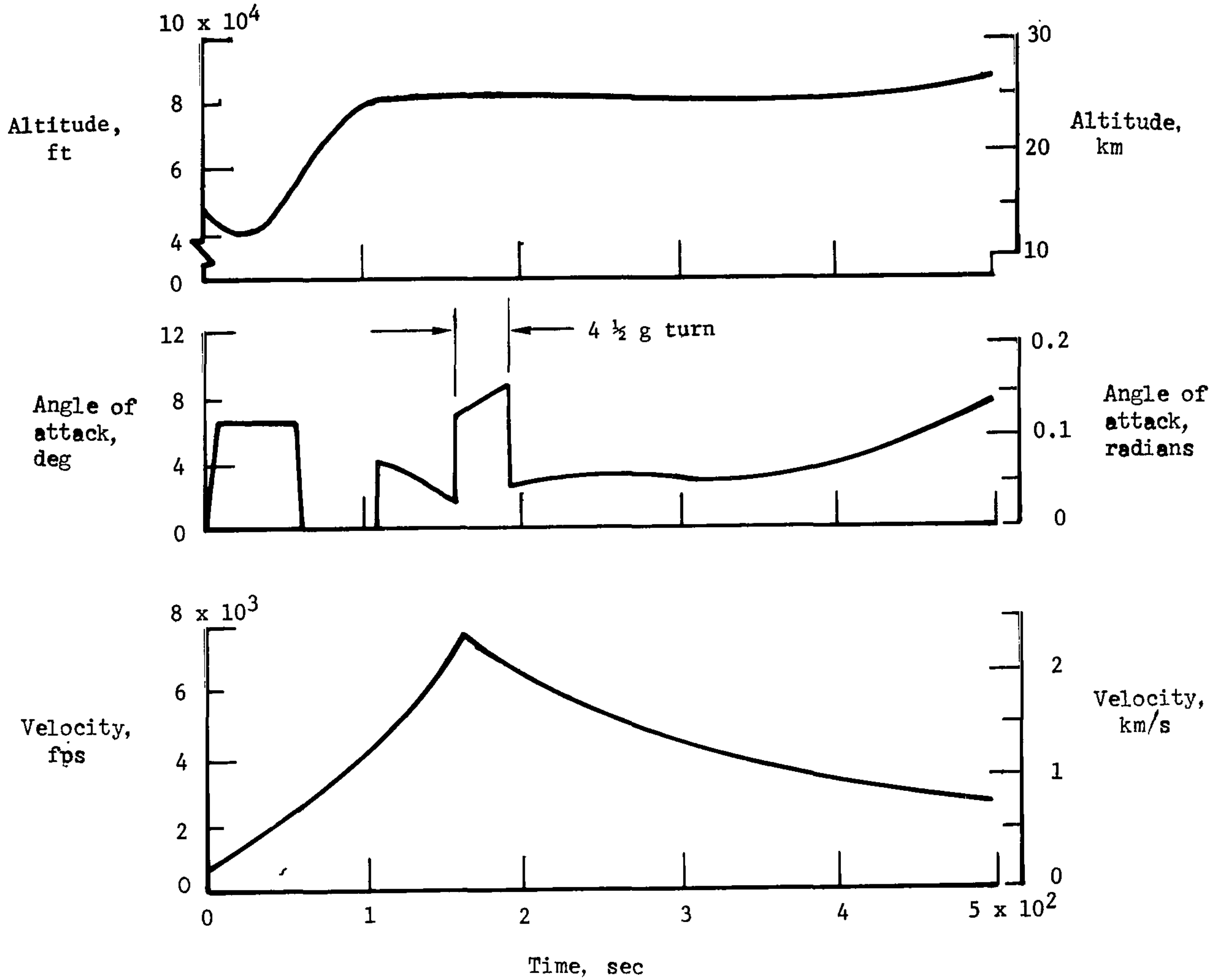

Figure 2.- Variation of flight conditions along vehicle flight path.

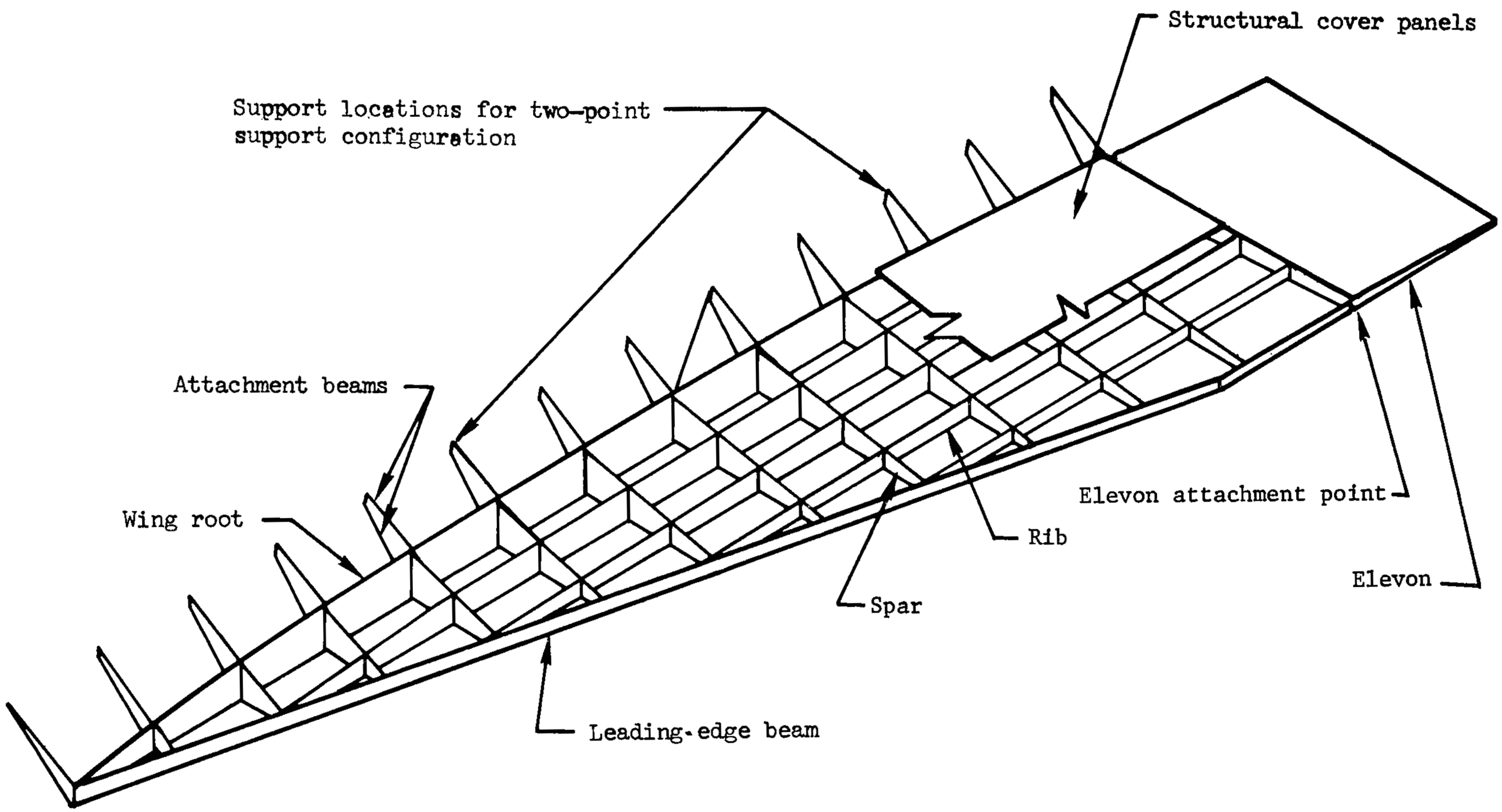

Figure 3.- Layout of structural configurations.

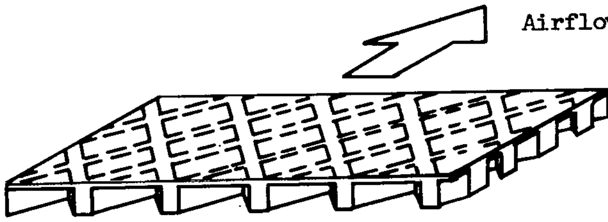

(a) Waffle.

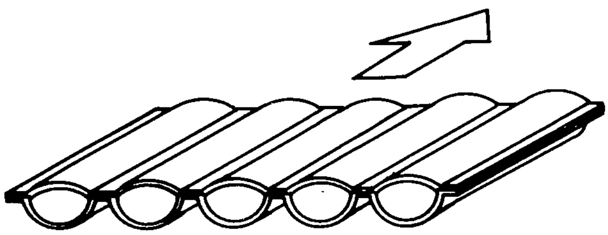

(b) Beaded-skin and circular-arc corrugation.

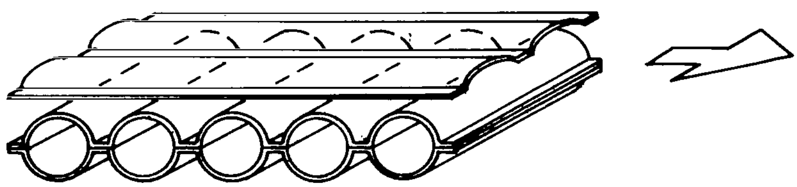

(c) Tubular.

Figure 4.- Structural panels considered in analysis.

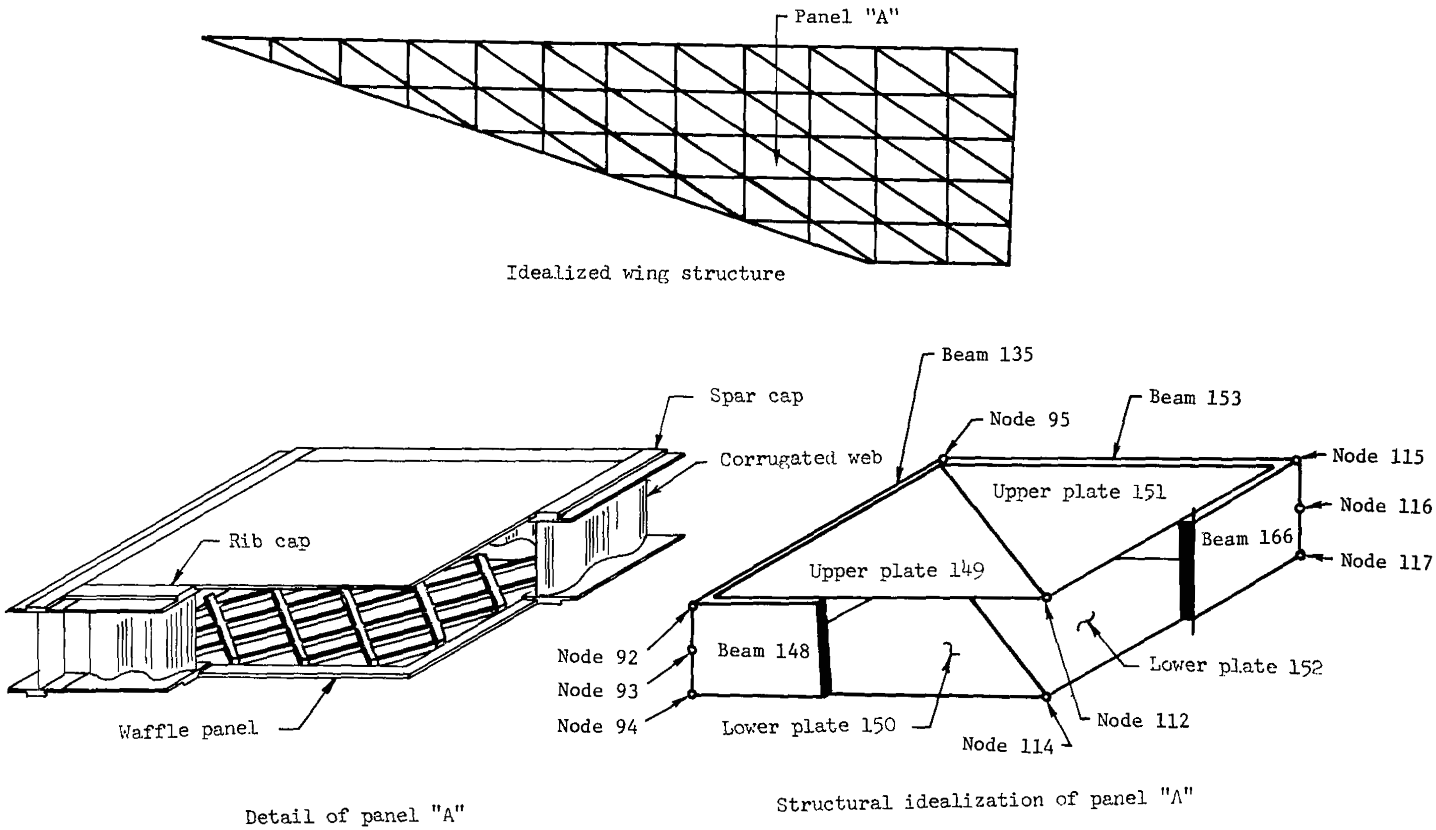

Figure 5.- Typical structural idealization of wing structure.

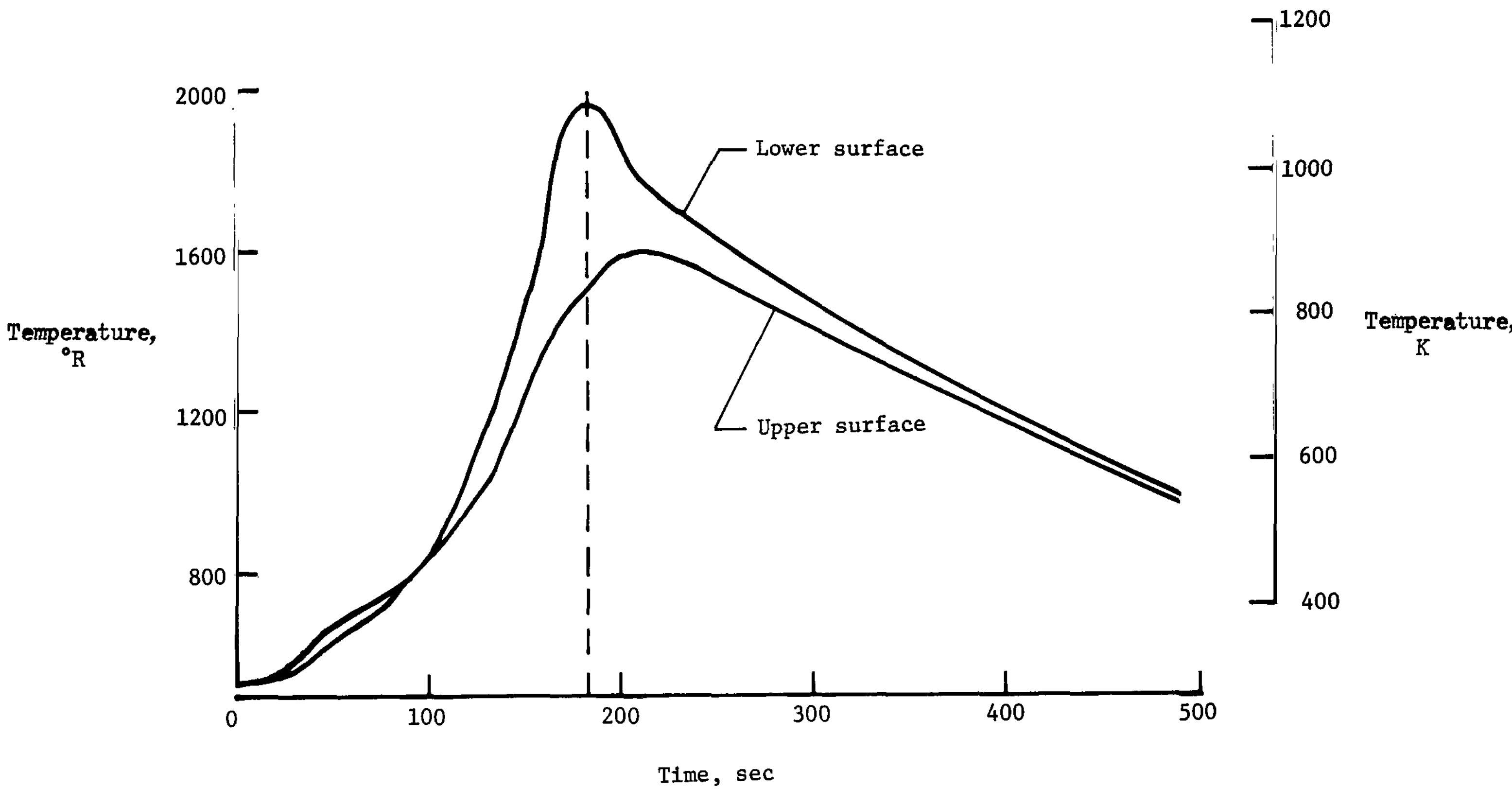

(a) Configuration 1.

Figure 6.- Typical temperature history of structural panels 11.6 feet (3.54 meters) aft of leading edge on root chord. Dashed lines indicate flight time for design conditions.

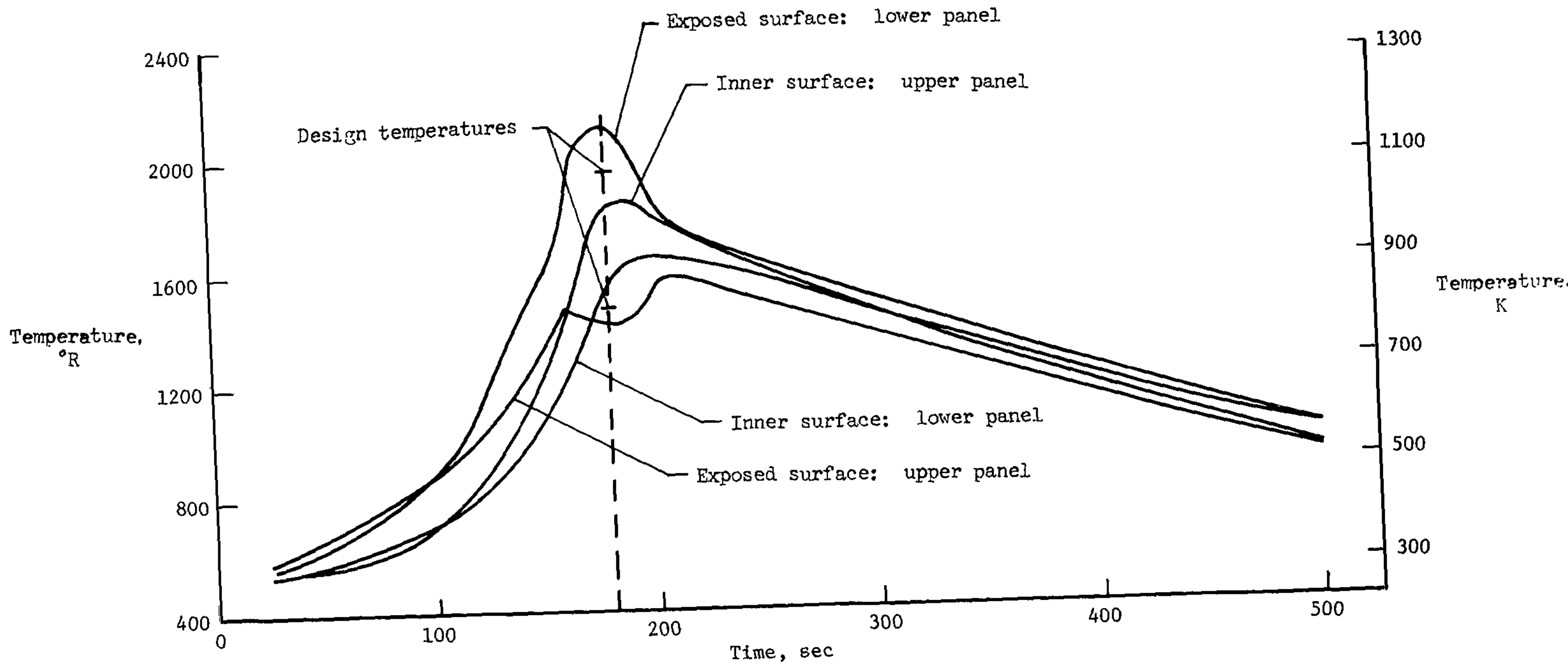

(b) Configurations 2 and 3.

Figure 6.- Continued.

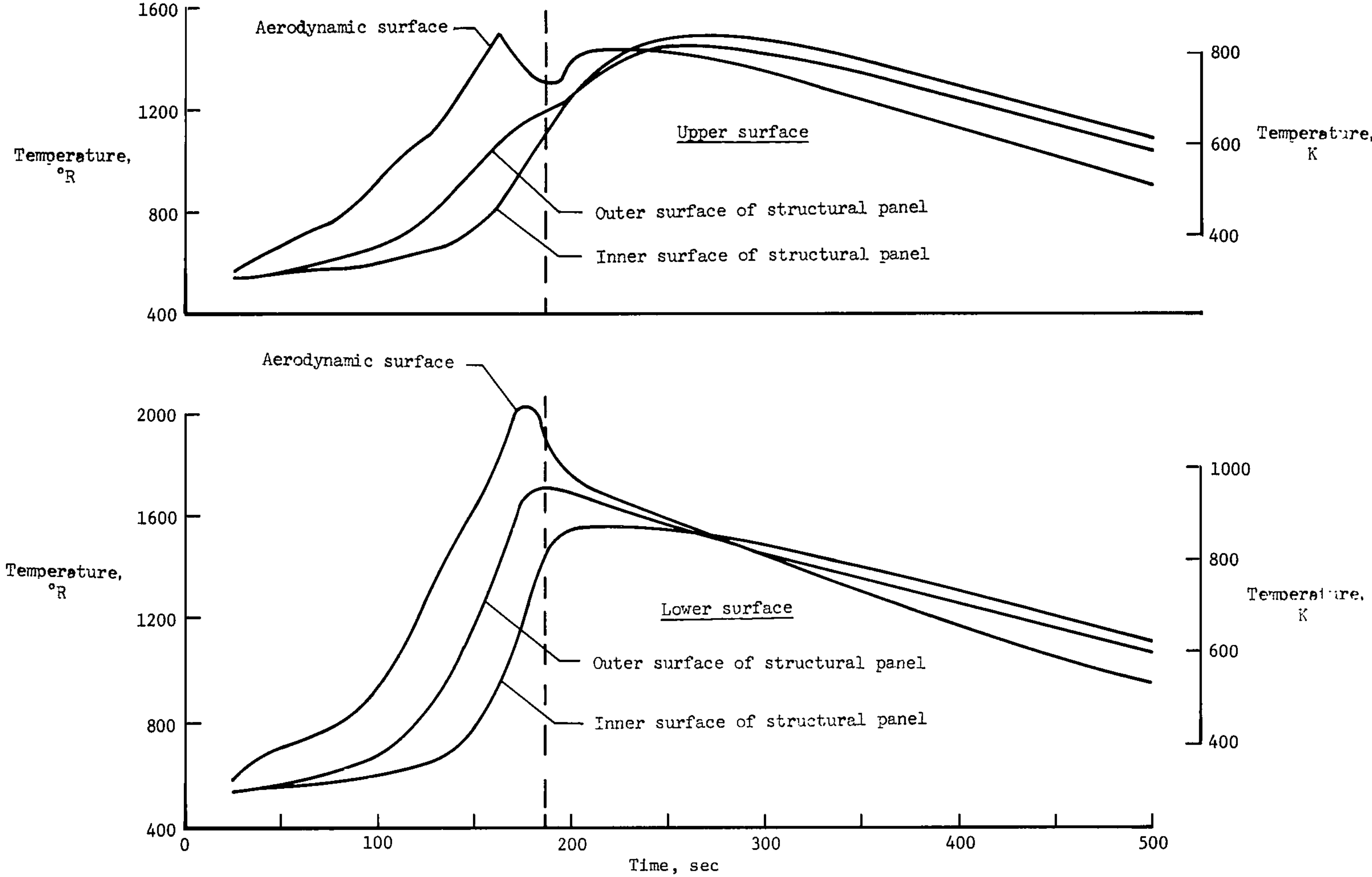

(c) Configurations 4 and 5.

Figure 6.- Concluded.

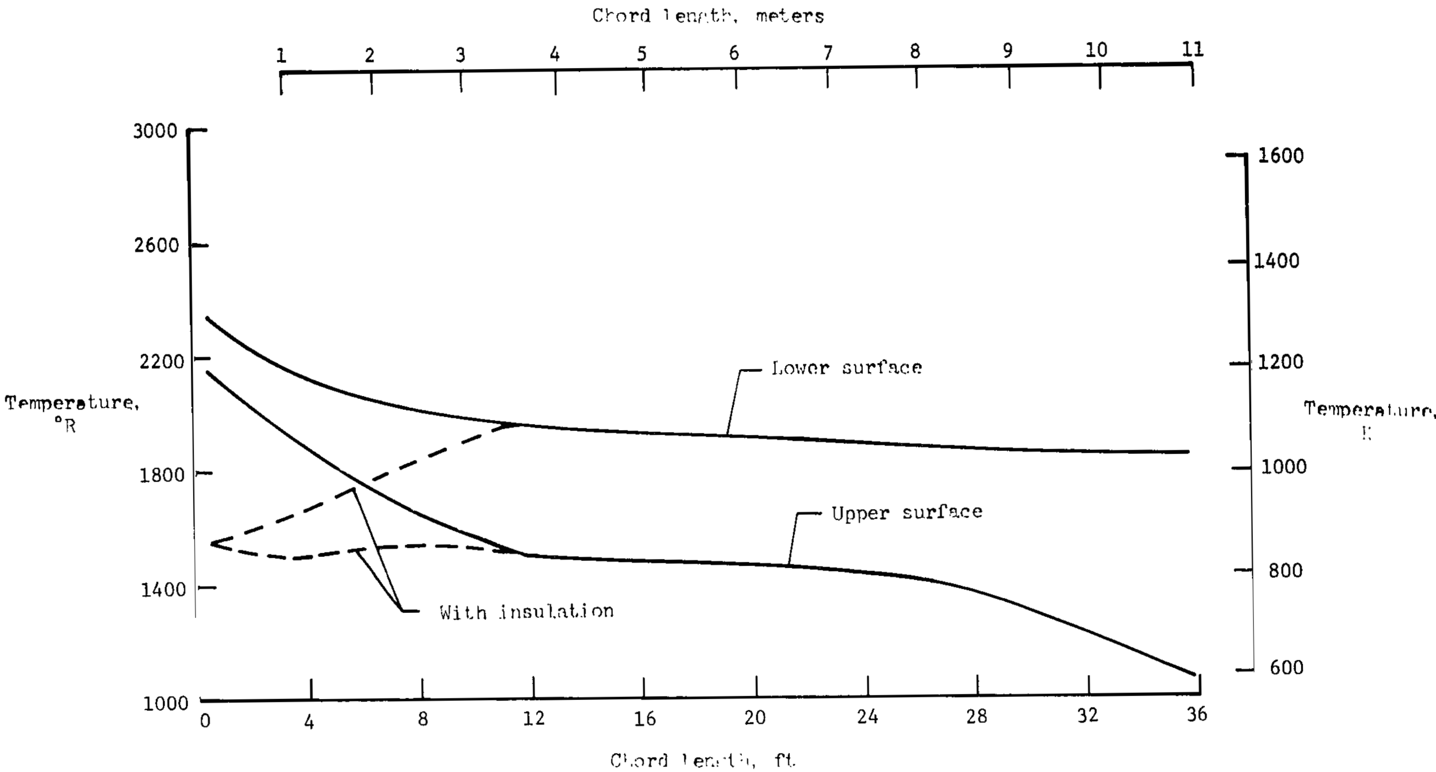

(a) Configurations 1, 2, and 3.

Figure 7.- Chordwise temperature distributions at root chord.

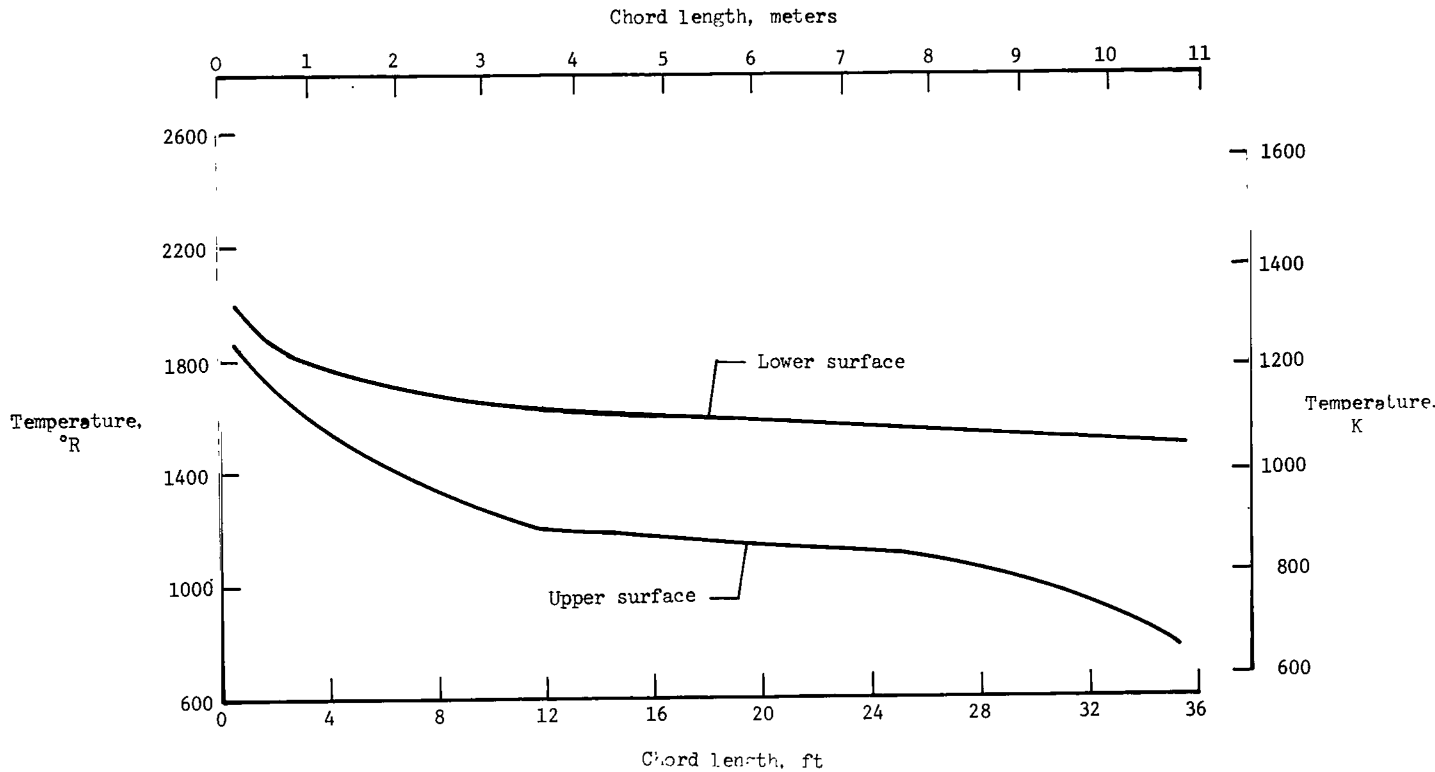

(b) Configuration 4.

Figure 7.- Continued.

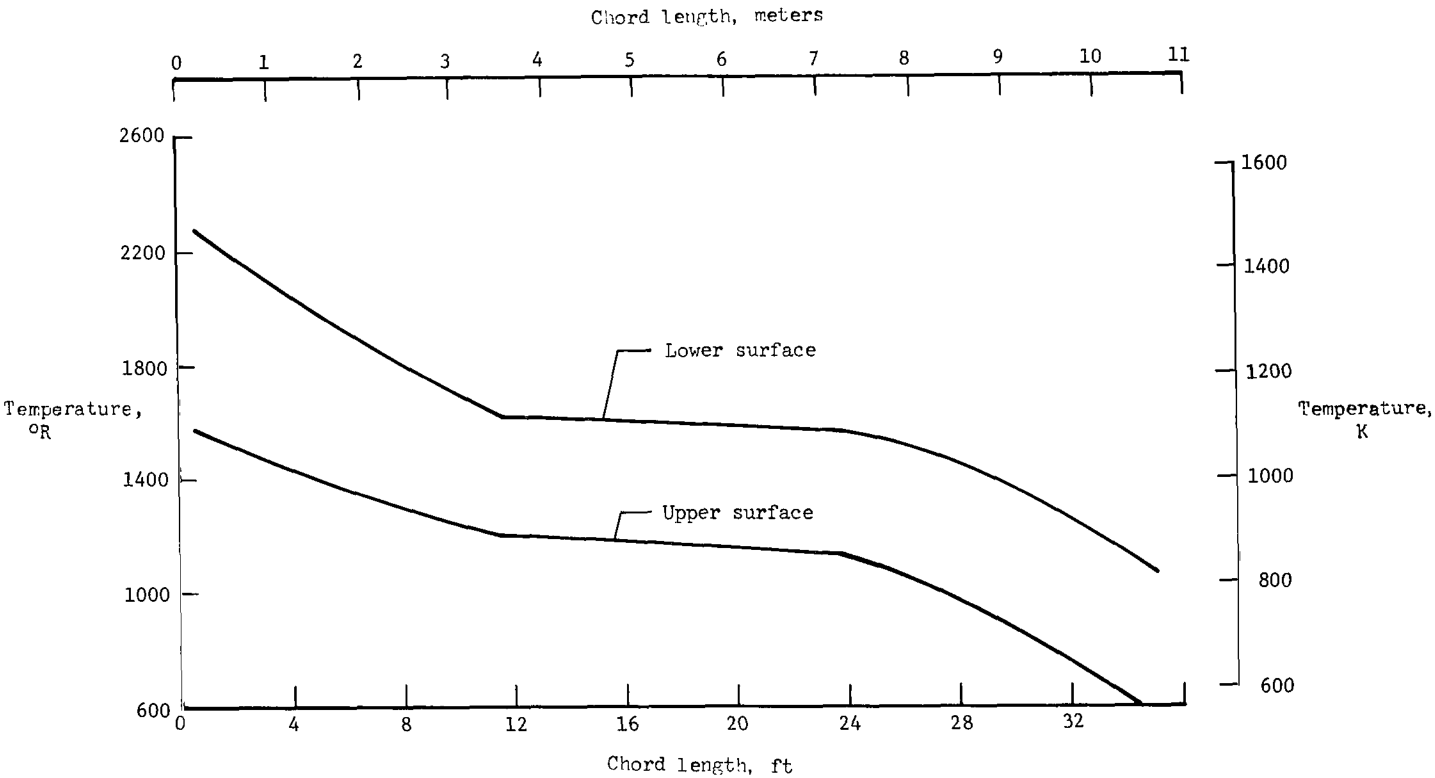

(c) Configuration 5.

Figure 7.- Concluded.

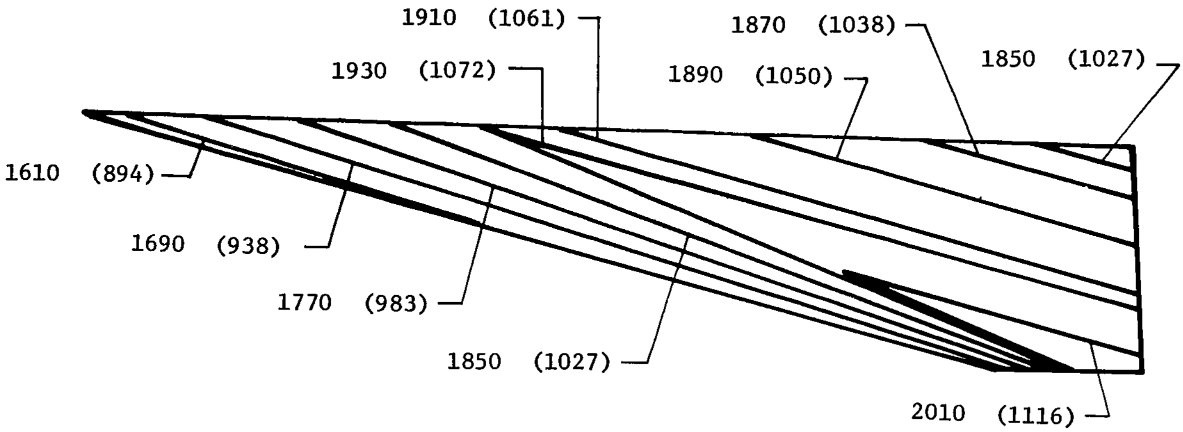

(a) Lower surface.

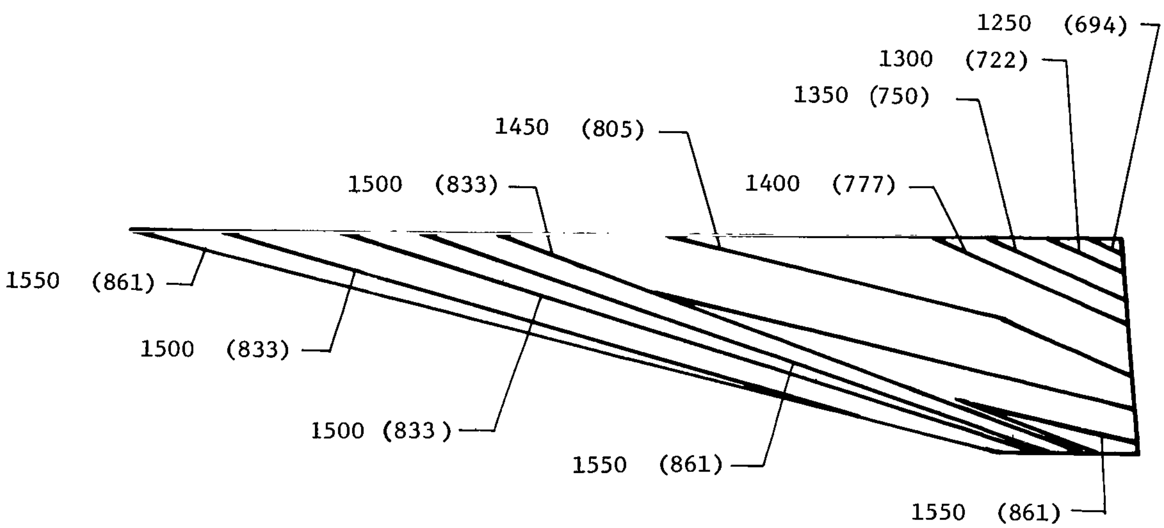

(b) Upper surface.

Figure 8.- Temperature distribution (^{o}R (K)) in structural panels of configurations 1, 2, and 3.

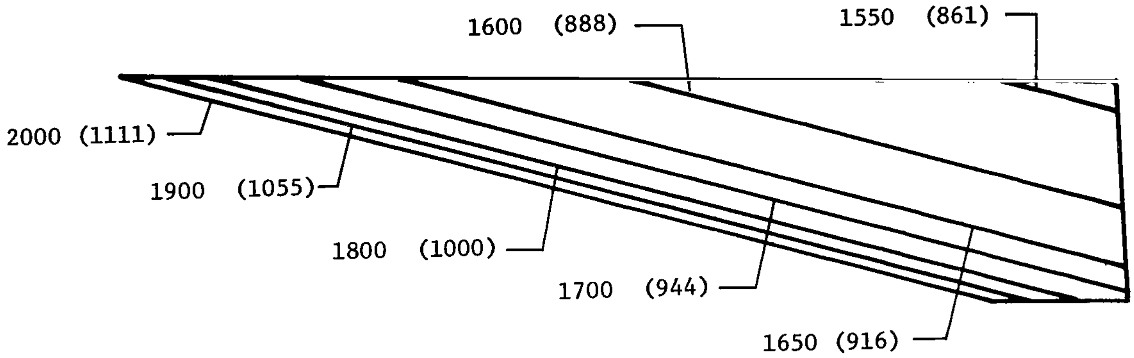

(a) Lower surface.

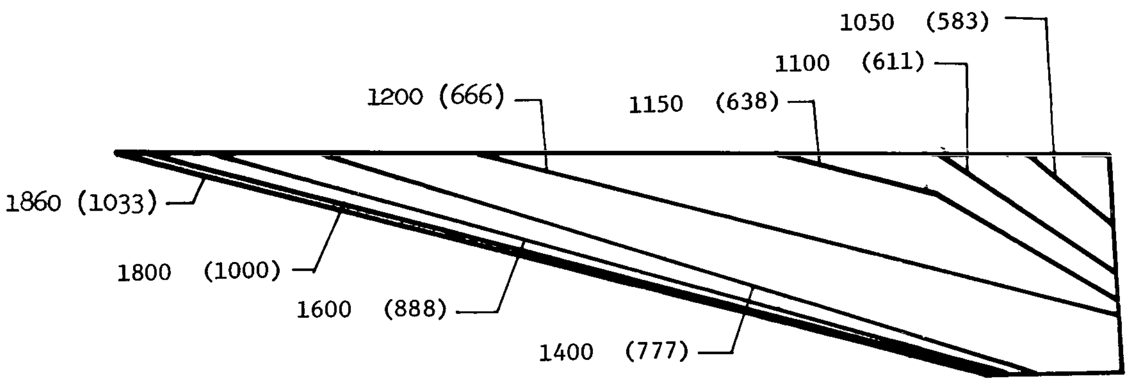

(b) Upper surface.

Figure 9.- Temperature distribution (^{o}R (K)) in structural panels of configuration 4.

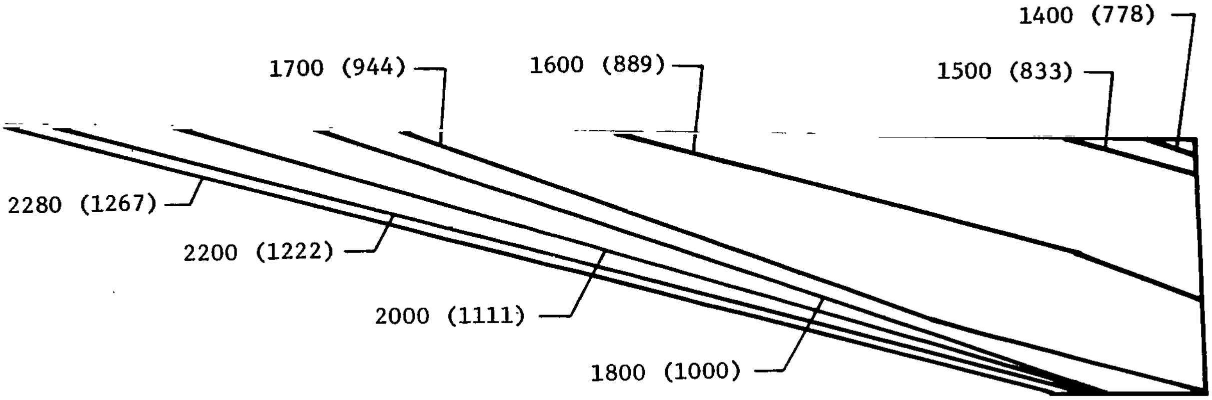

(a) Lower surface.

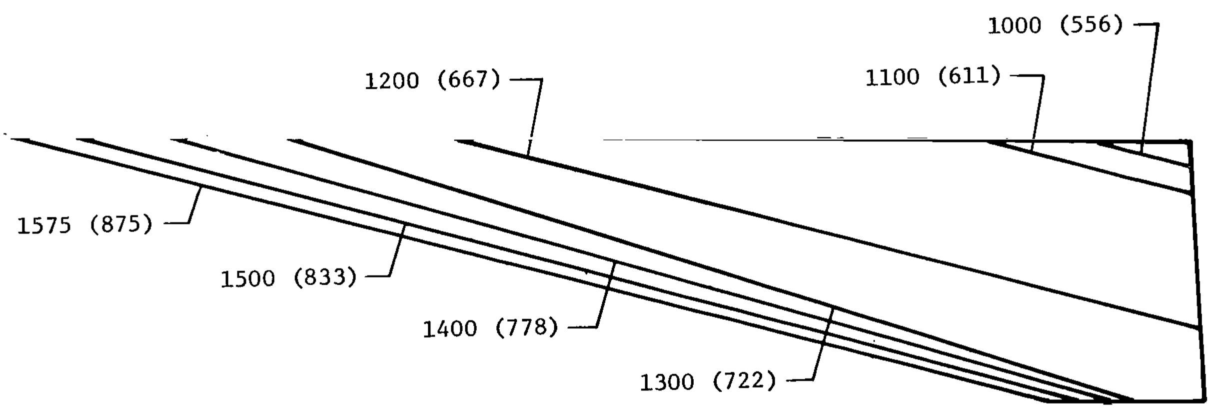

(b) Upper surface.

Figure 10.- Temperature distribution ($^{\circ}$R (K)) in structural panels of configuration 5.

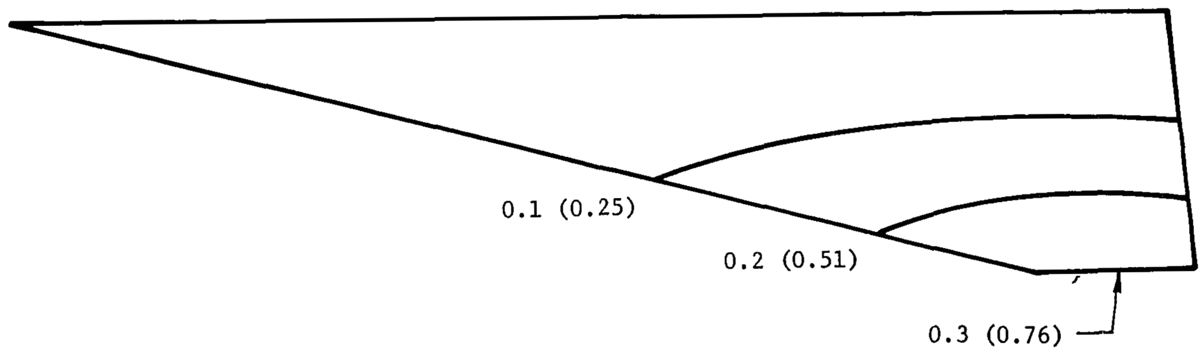

(a) Configuration 1.

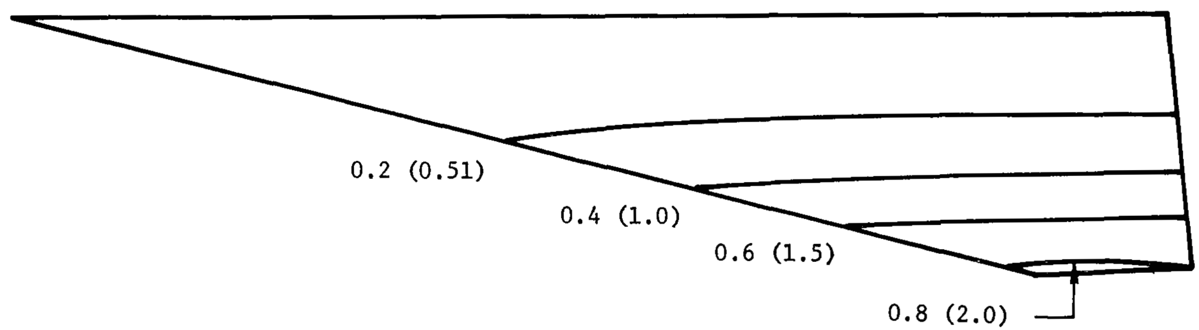

(b) Configuration 2.

Figure 11.- Vertical deflections (inches (cm)) of wing due to airloads plus inertia forces.

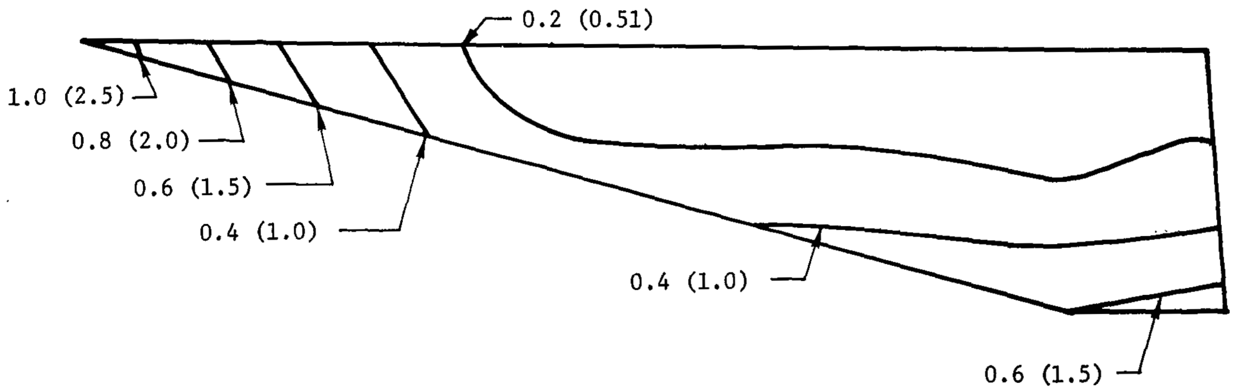

(c) Configuration 3.

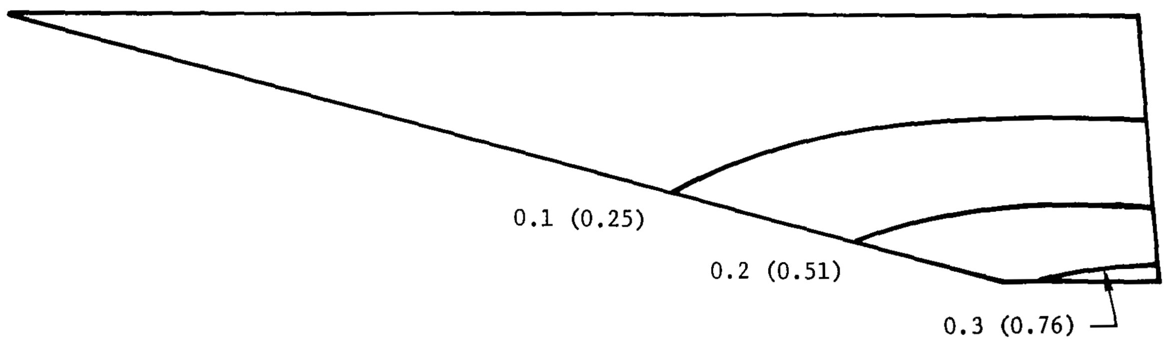

(d) Configuration 4.

Figure 11.- Continued.

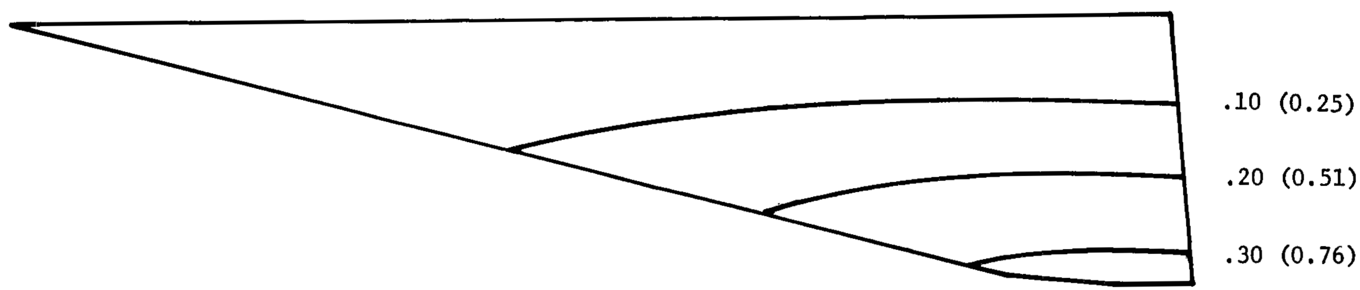

(e) Configuration 5.

Figure 11.- Concluded.

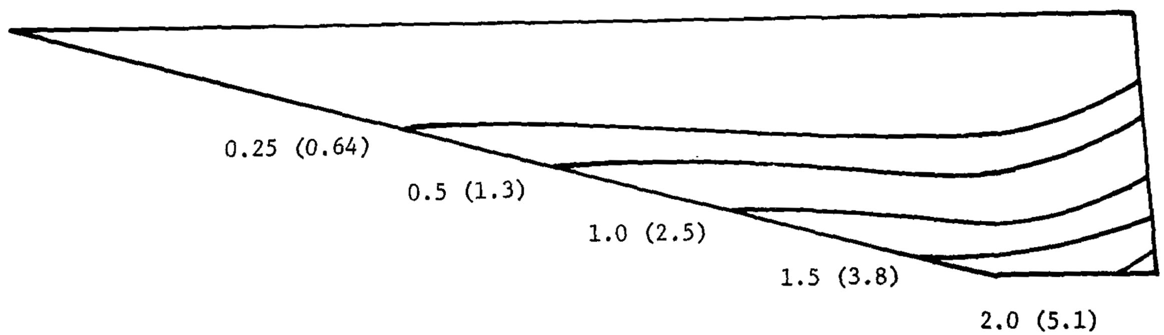

(a) Configuration 1.

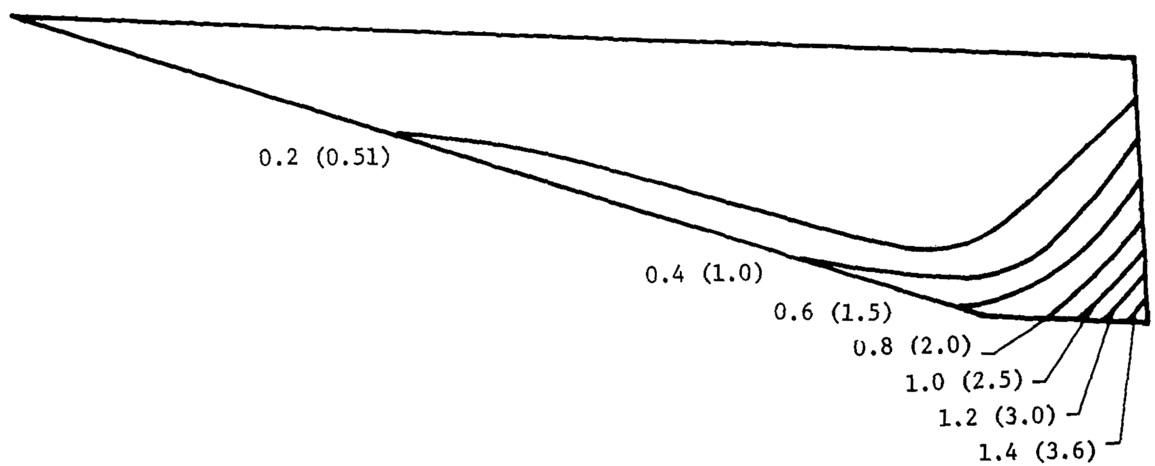

(b) Configuration 2.

Figure 12.- Wing vertical deflections (inches (cm)) due to temperature distribution.

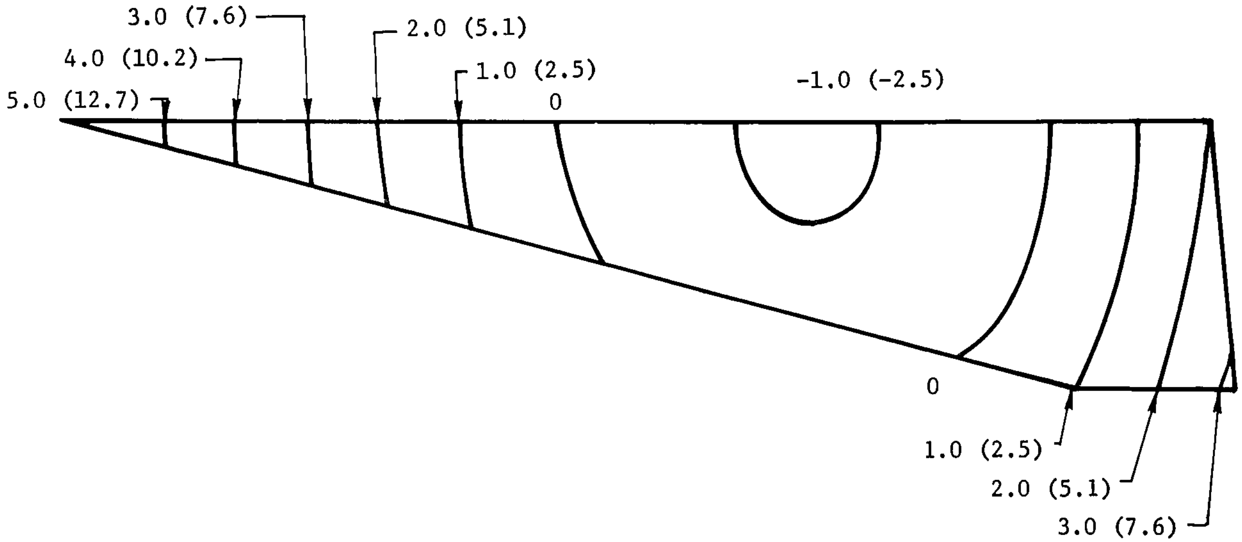

(c) Configuration 3.

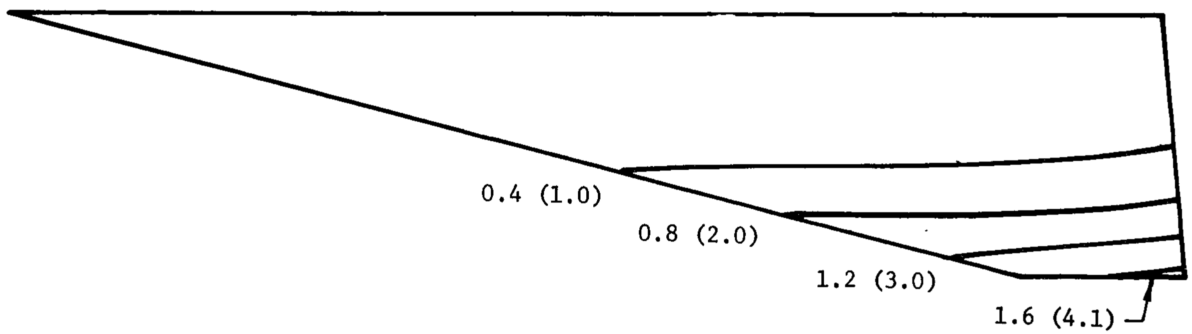

(d) Configuration 4.

Figure 12.- Continued.

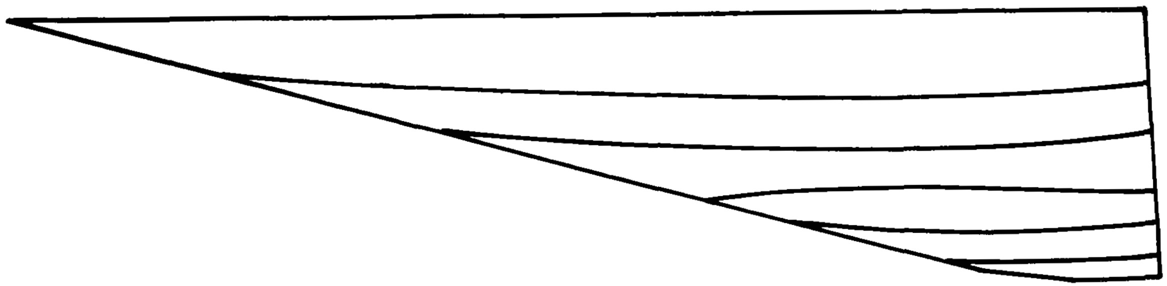

(e) Configuration 5.

Figure 12.- Concluded.

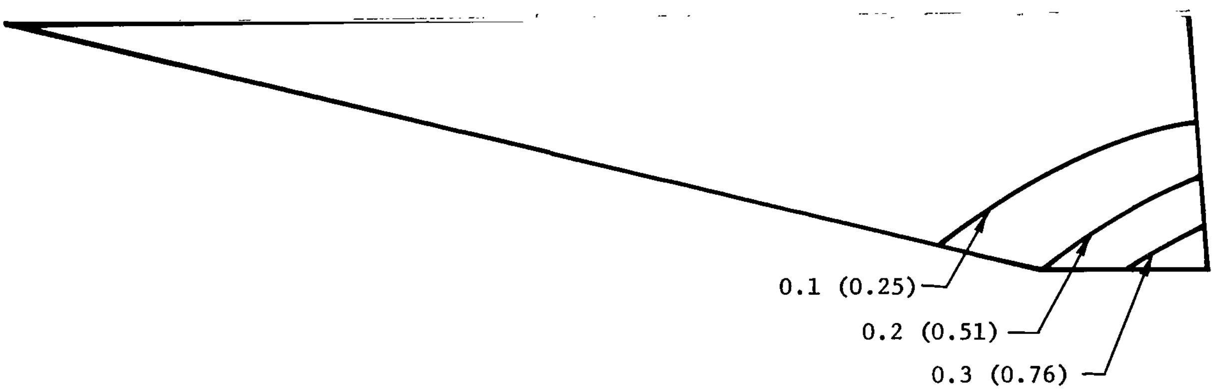

(a) Configuration 1.

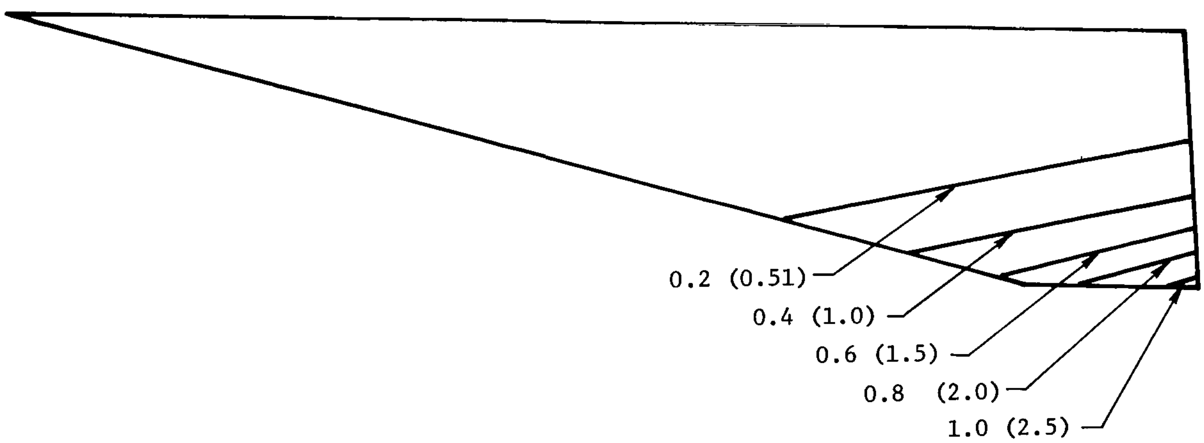

(b) Configuration 2.

Figure 13.- Wing vertical deflections (inches (cm)) due to elevon load.

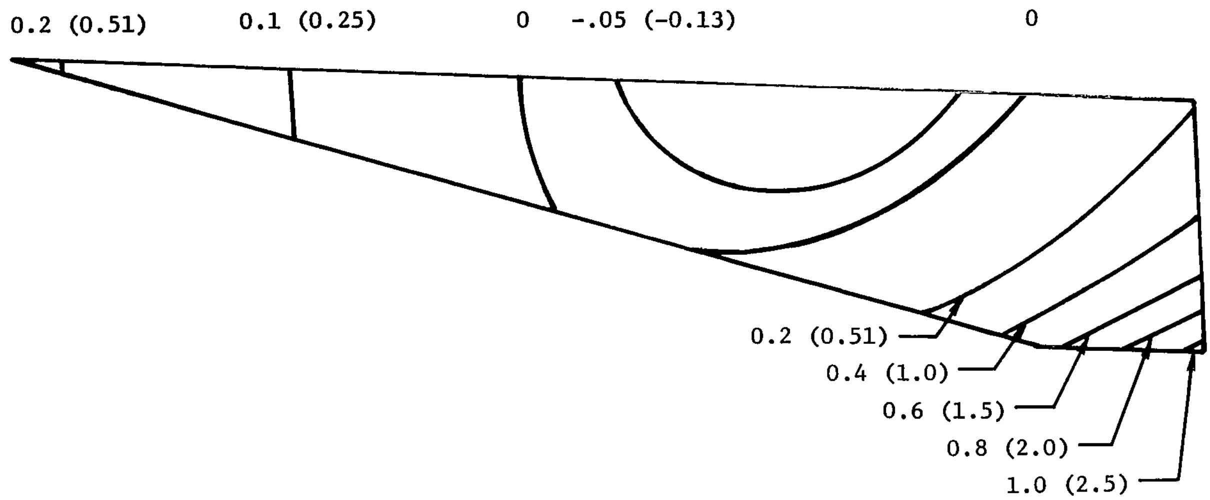

(c) Configuration 3.

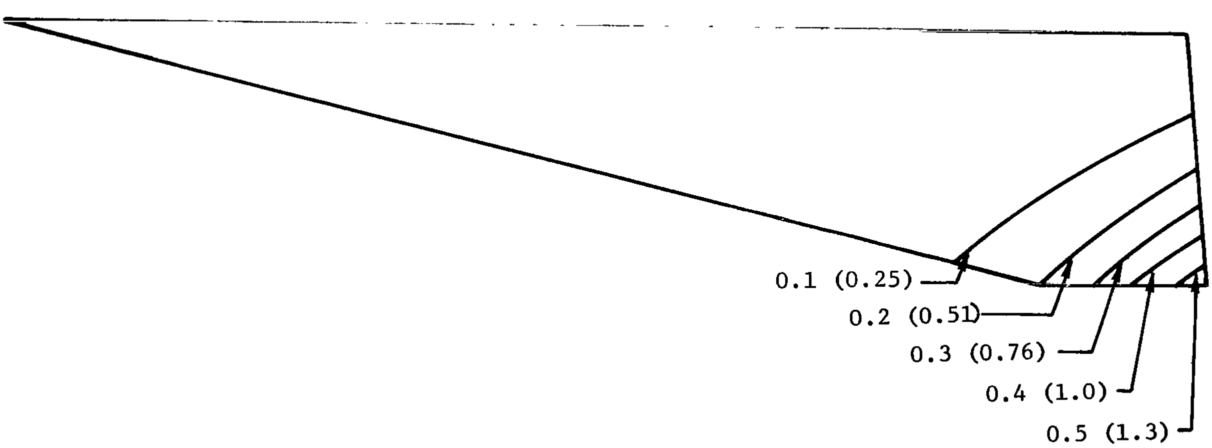

(d) Configurations 4 and 5.

Figure 13.- Concluded.

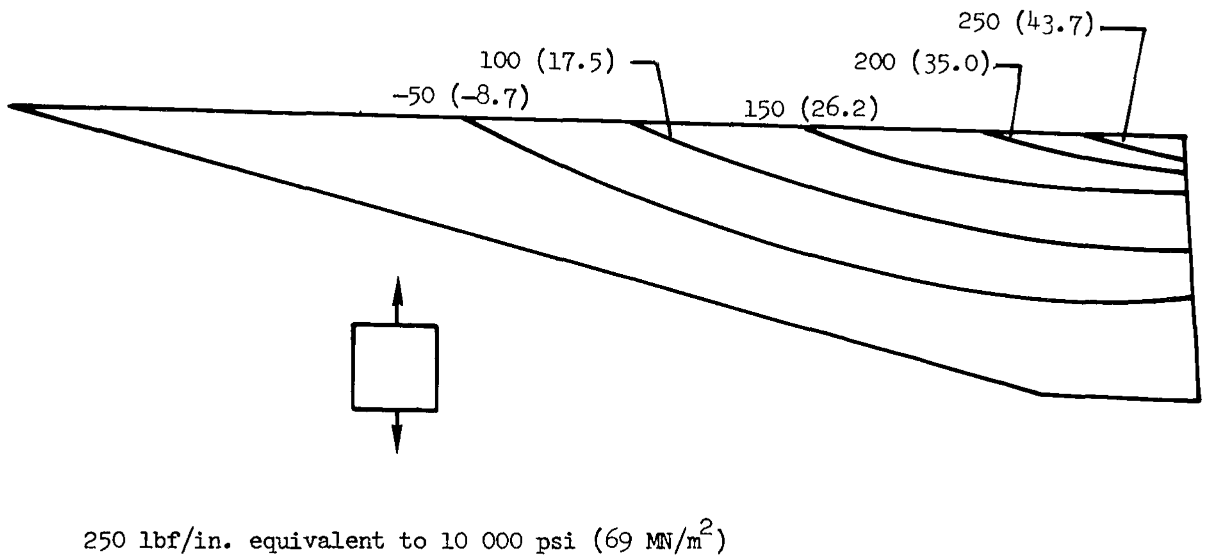

(a) Configuration 1; N_Y stress resultant.

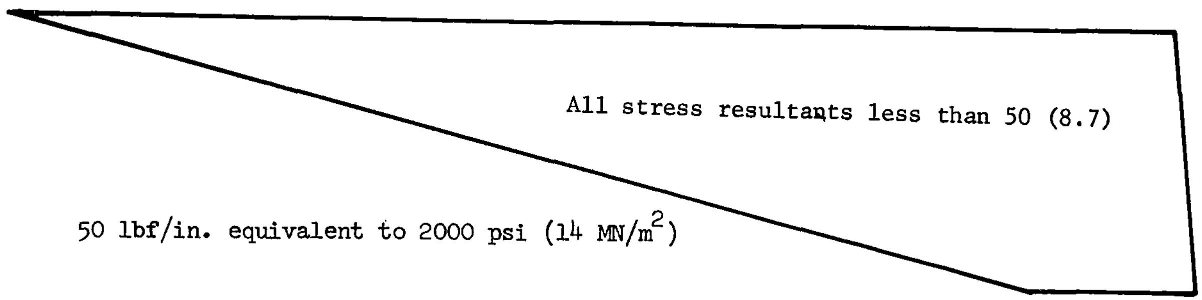

(b) Configuration 2.

Figure 14.- Stress resultants (lbf/in. (kN/m)) in lower cover panels due to airloads plus inertia forces.

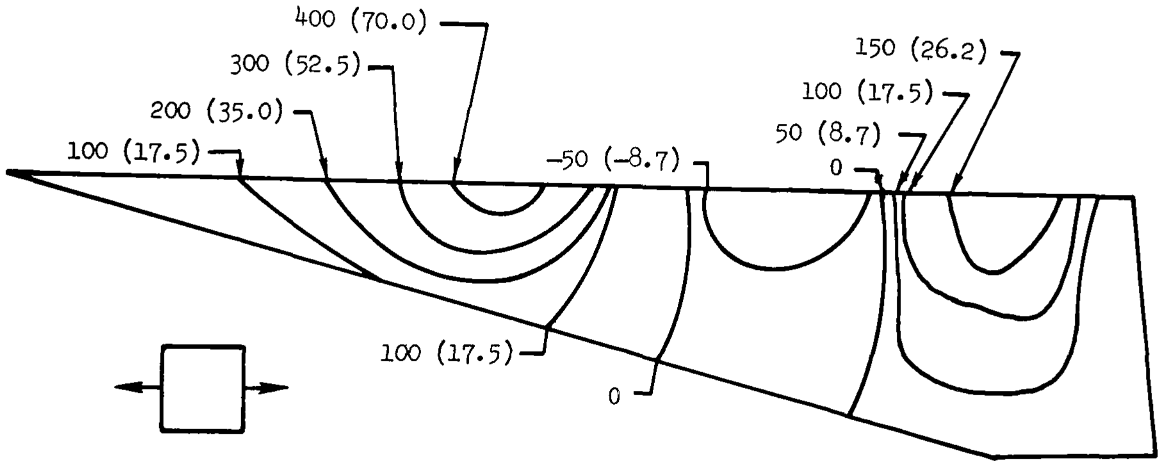

400 lbf/in. equivalent to 13 000 psi (90 MN/m^2)

(c) Configuration 3; N_X stress resultant.

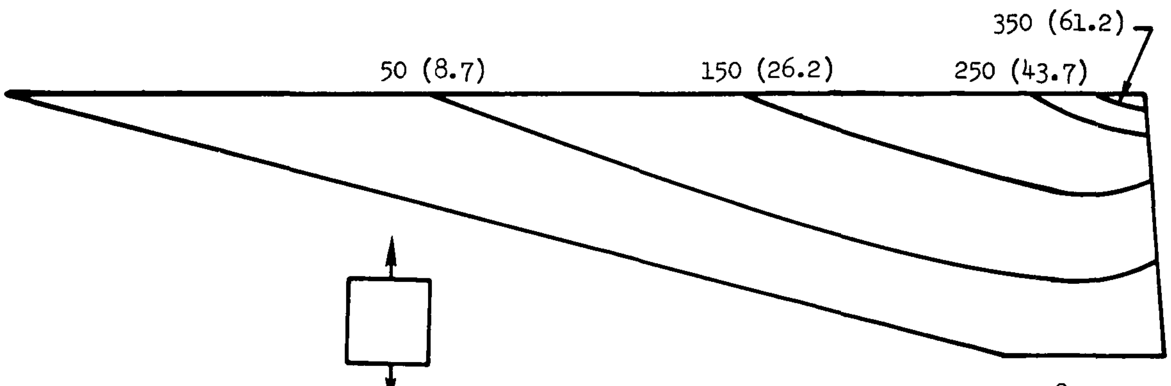

350 lbf/in. equivalent to 12 000 psi (83 MN/m^2)

(d) Configuration 4; N_Y stress resultant.

Figure 14.- Continued.

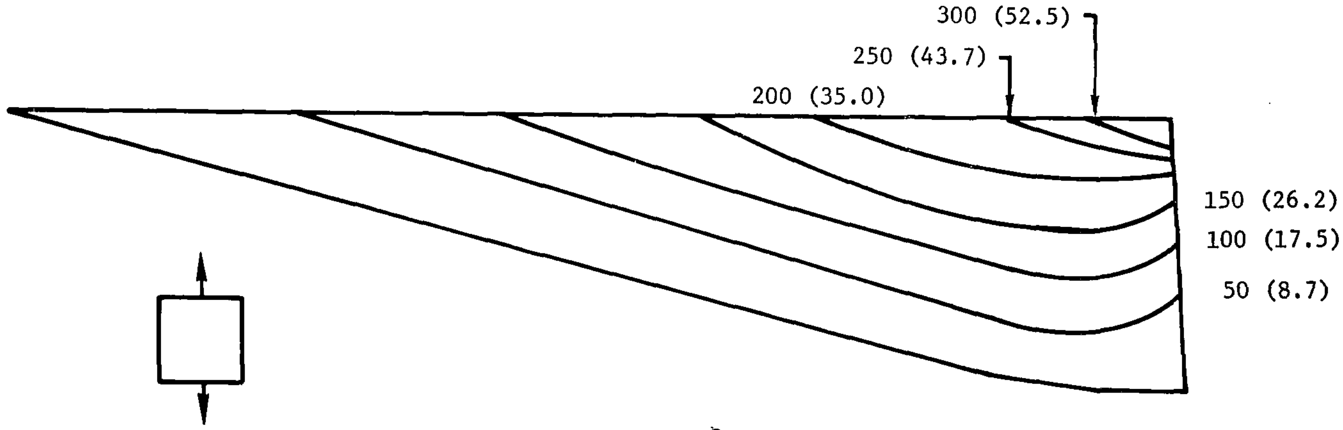

(e) Configuration 5; N_Y stress resultant.

Figure 14.- Concluded.

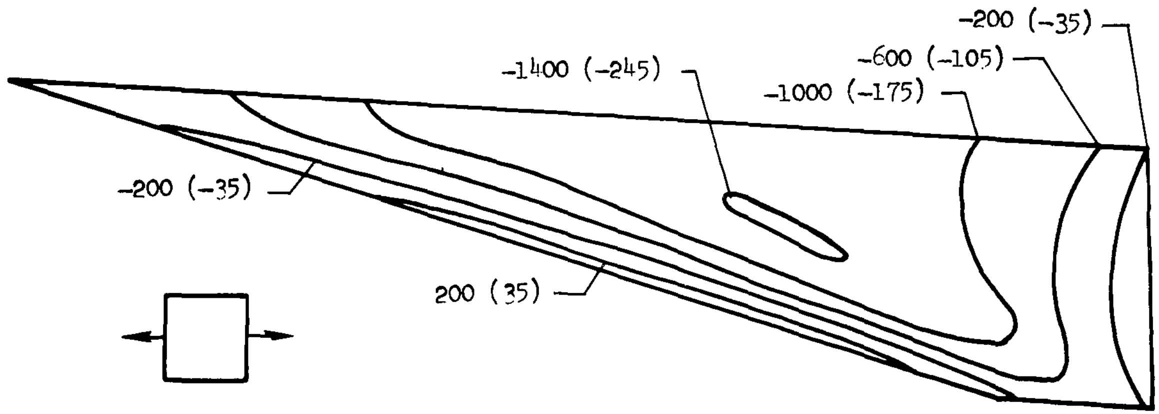

1400 lbf/in. equivalent to 56 000 psi (386 MN/m^2)

(a) Configuration 1; N_X stress resultant.

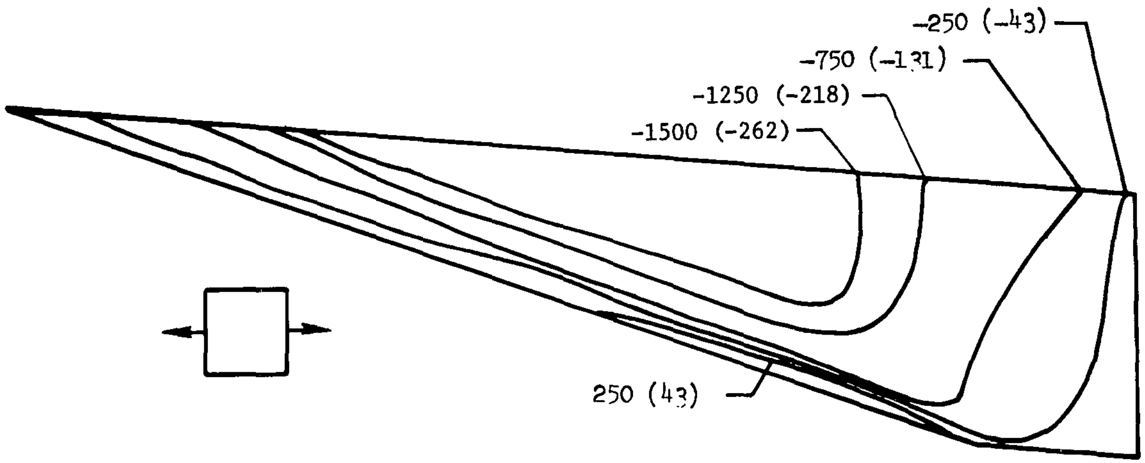

1500 lbf/in. equivalent to 47 000 psi (324 MN/m^2)

(b) Configuration 2; N_X stress resultant.

Figure 15.- Stress resultants (lbf/in. (kN/m)) in lower cover panels due to temperature distribution.

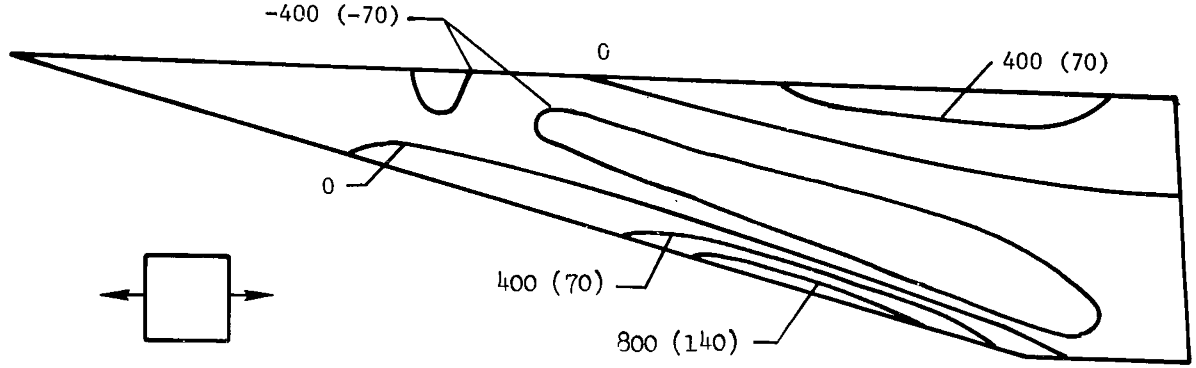

800 lbf/in. equivalent to 25 000 psi (172 MN/m^2).

(c) Configuration 3; N_X stress resultant.

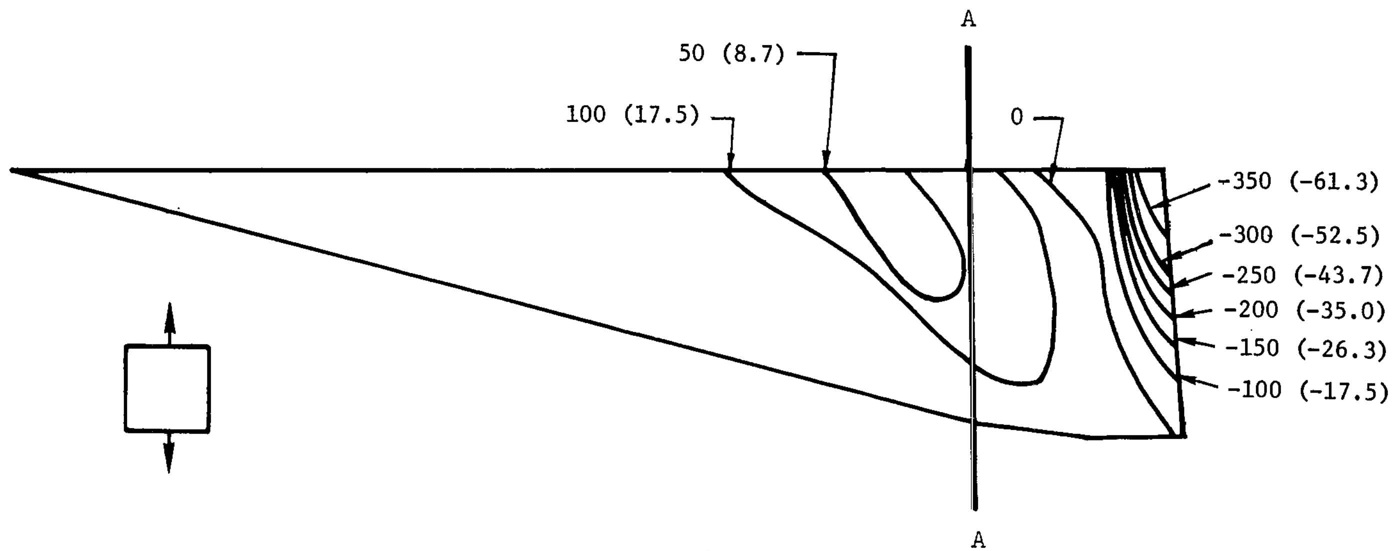

350 lbf/in. equivalent to 12 000 psi (83 MN/m^2)

(d) Configuration 4; N_Y stress resultant.

Figure 15.- Continued.

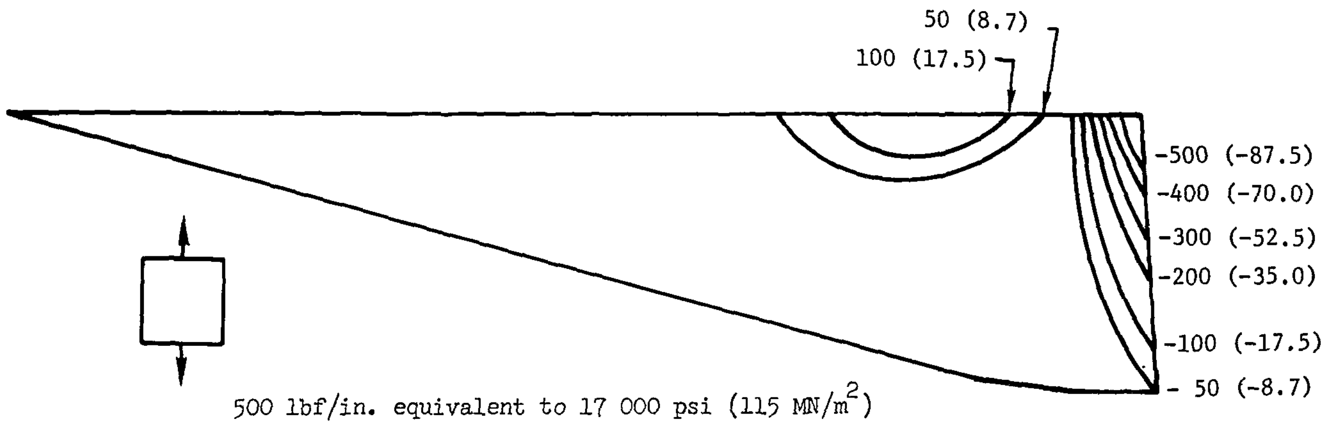

(e) Configuration 5; N_Y stress resultant.

Figure 15.- Concluded.

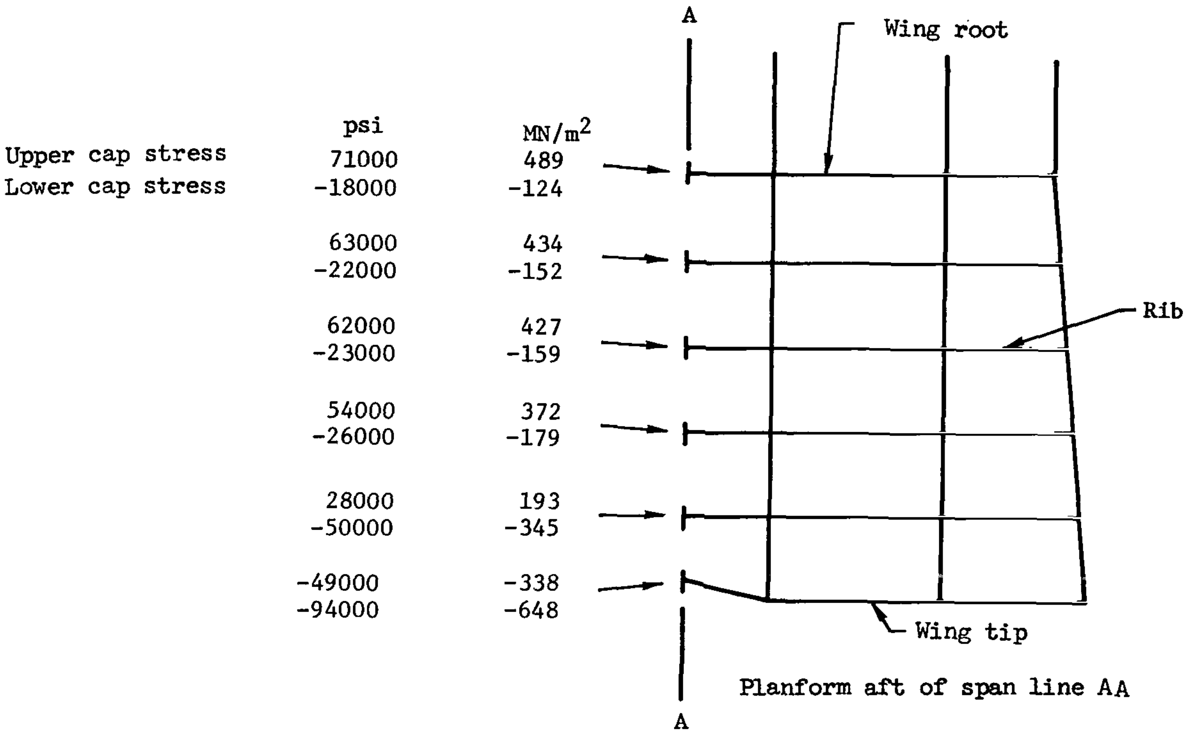

(a) Configuration 4 with beam-cap temperatures equal to temperature of adjacent cover panel.

Figure 16.- Spanwise distribution of thermal stress in rib caps along span line AA. (See fig. 15(d).)

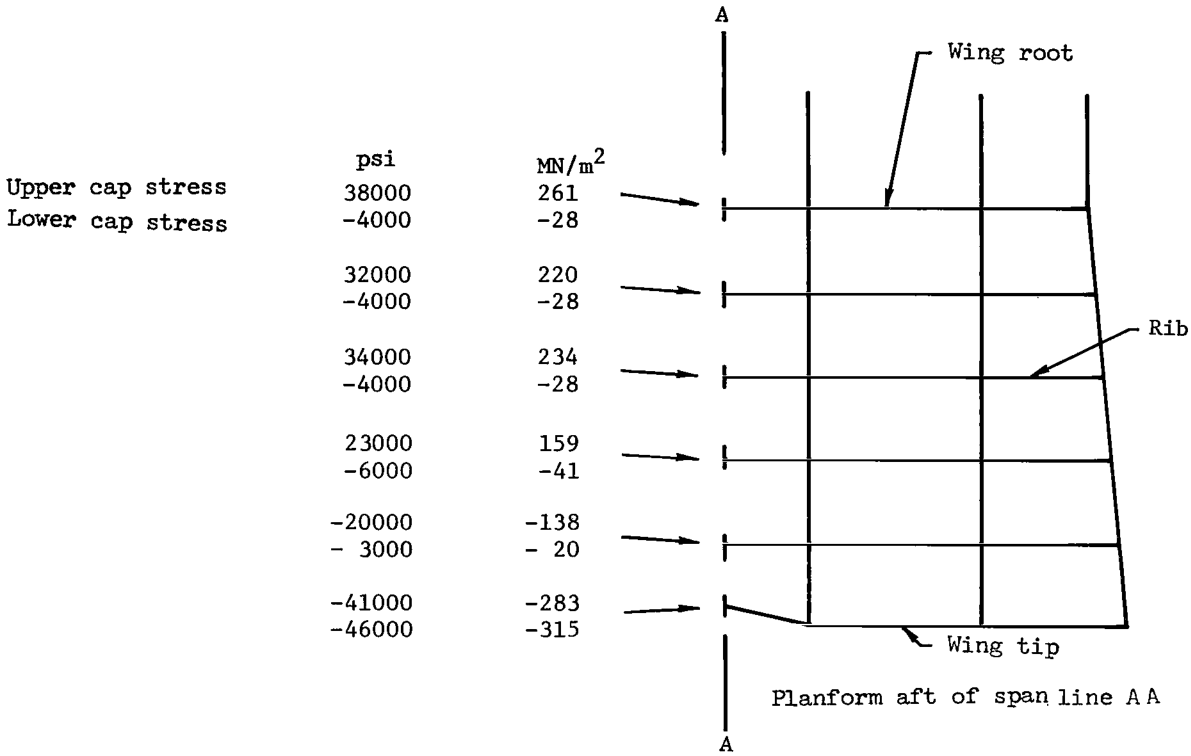

(b) Configuration 4 with thermal protection for beam caps.

Figure 16.- Continued.

	psi	MN/m^2
Upper cap stress	69000	476
Lower cap stress	-10000	-69
	66000	455
	-17000	-117
	60000	414
	-17000	-117
	54000	372
	-23000	-159
	33000	228
	-63000	-434
	29000	200
	-184000	-1269

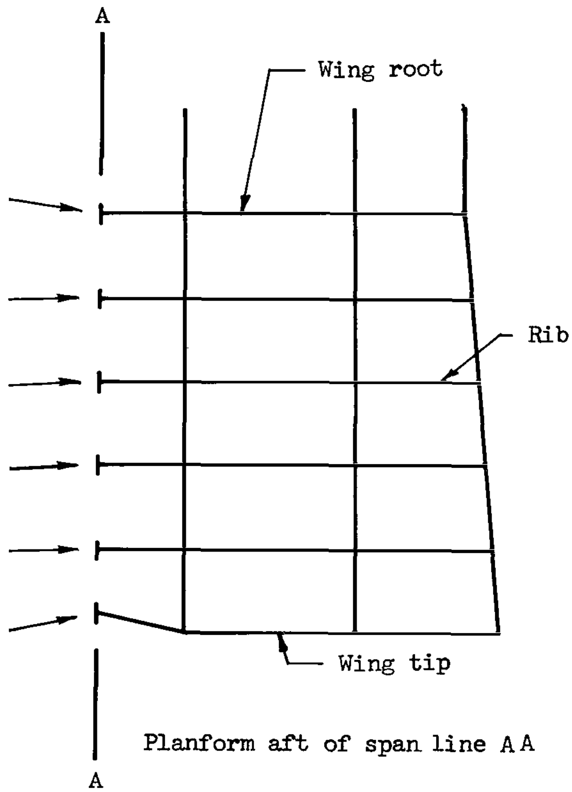

(c) Configuration 5 with beam-cap temperatures equal to temperature of adjacent cover panel.

Figure 16.- Concluded.

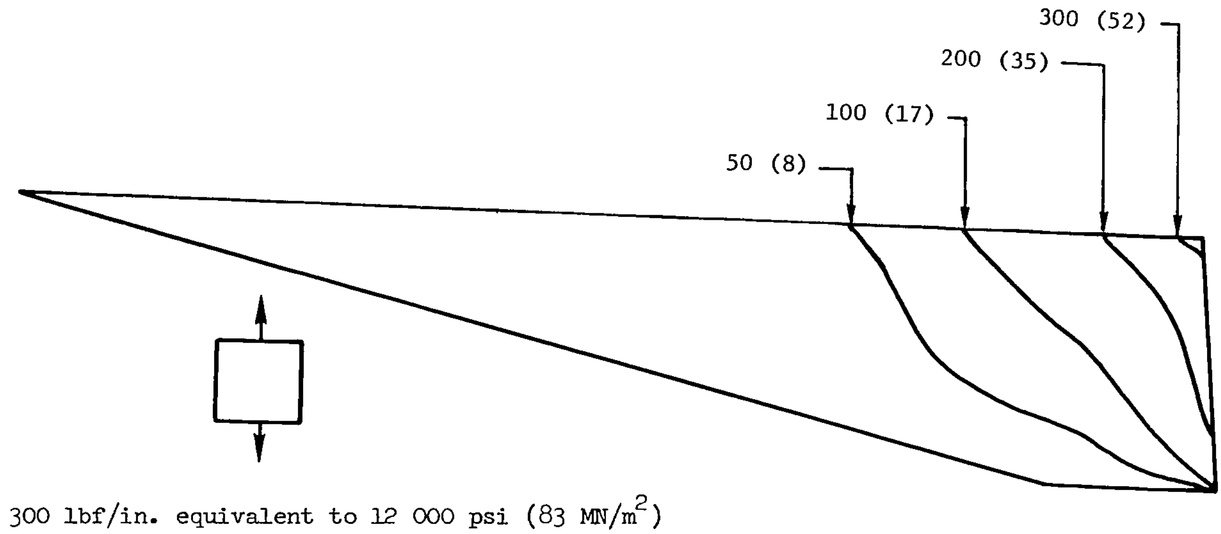

(a) Configuration 1; N_Y stress resultants.

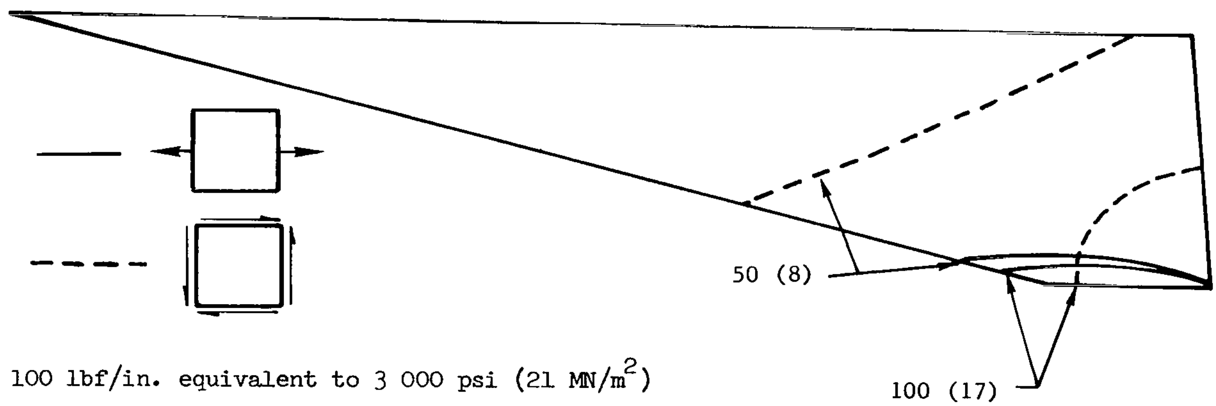

(b) Configuration 2; N_X and N_{XY} stress resultants.

Figure 17.- Stress resultants (lbf/in. (kN/m)) in lower cover panels due to elevon load.

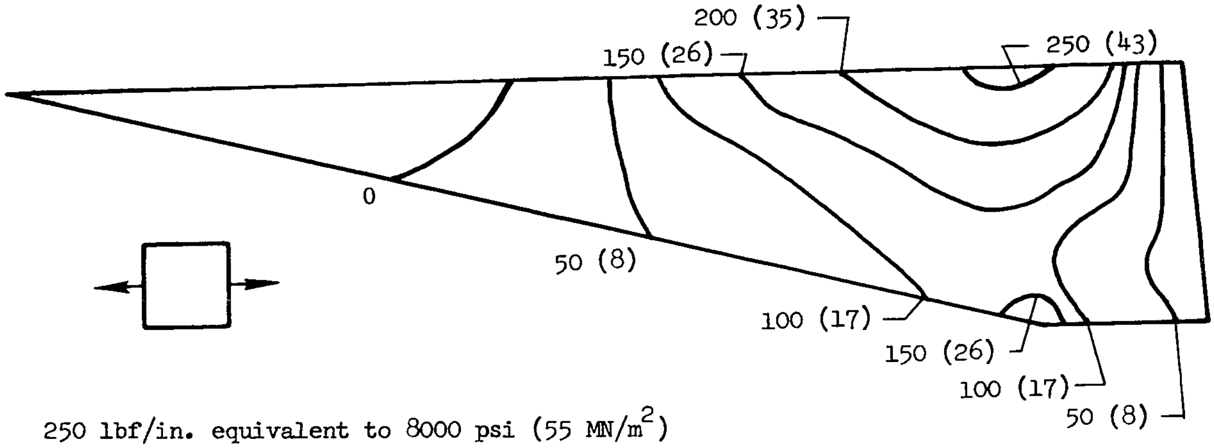

250 lbf/in. equivalent to 8000 psi (55 MN/m^2)

(c) Configuration 3; N_X stress resultants.

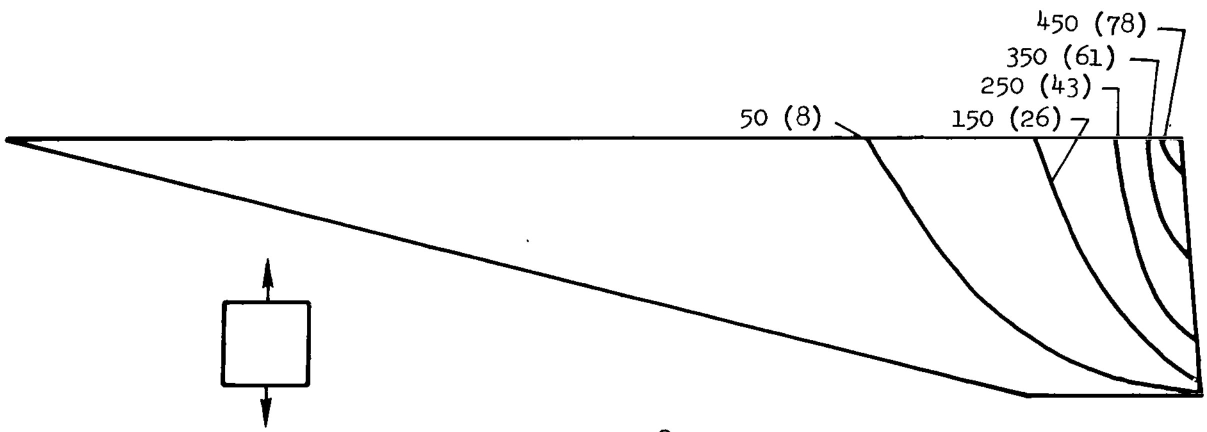

450 lbf/in. equivalent to 15 000 psi (103 MN/m^2)

(d) Configuration 4; N_Y stress resultants.

Figure 17.- Concluded.

NASA-Langley, 1971 —— 32 L-6666

NATIONAL AERONAUTICS AND SPACE ADMINISTRATION
WASHINGTON, D. C. 20546

OFFICIAL BUSINESS

FIRST CLASS MAIL

POSTAGE AND FEES PAI
NATIONAL AERONAUTICS
SPACE ADMINISTRATIO

```
03U 001 57  51 3DS        71012  00903
AIR FORCE WEAPONS LABORATORY /WLOL/
KIRTLAND AFB, NEW MEXICO  87117

ATT E. LOU BOWMAN, CHIEF,TECH. LIBRARY
```

POSTMASTER: If Undeliverable (Section 1 Postal Manual) Do Not Re

"The aeronautical and space activities of the United States shall be conducted so as to contribute . . . to the expansion of human knowledge of phenomena in the atmosphere and space. The Administration shall provide for the widest practicable and appropriate dissemination of information concerning its activities and the results thereof."

—NATIONAL AERONAUTICS AND SPACE ACT OF 1958

NASA SCIENTIFIC AND TECHNICAL PUBLICATIONS

TECHNICAL REPORTS: Scientific and technical information considered important, complete, and a lasting contribution to existing knowledge.

TECHNICAL NOTES: Information less broad in scope but nevertheless of importance as a contribution to existing knowledge.

TECHNICAL MEMORANDUMS: Information receiving limited distribution because of preliminary data, security classification, or other reasons.

CONTRACTOR REPORTS: Scientific and technical information generated under a NASA contract or grant and considered an important contribution to existing knowledge.

TECHNICAL TRANSLATIONS: Information published in a foreign language considered to merit NASA distribution in English.

SPECIAL PUBLICATIONS: Information derived from or of value to NASA activities. Publications include conference proceedings, monographs, data compilations, handbooks, sourcebooks, and special bibliographies.

TECHNOLOGY UTILIZATION PUBLICATIONS: Information on technology used by NASA that may be of particular interest in commercial and other non-aerospace applications. Publications include Tech Briefs, Technology Utilization Reports and Technology Surveys.

Details on the availability of these publications may be obtained from:

SCIENTIFIC AND TECHNICAL INFORMATION OFFICE

NATIONAL AERONAUTICS AND SPACE ADMINISTRATION

Washington, D.C. 20546